Tellus (2000), 52B, 594–619
Printed in UK. All rights reserved

TELLUS
ISSN 0280–6509

Shipboard sunphotometer measurements of aerosol optical depth spectra and columnar water vapor during ACE-2, and comparison with selected land, ship, aircraft, and satellite measurements

By JOHN M. LIVINGSTON[1]*, VLADIMIR N. KAPUSTIN[2], BEAT SCHMID[3], PHILIP B. RUSSELL[4], PATRICIA K. QUINN[5], TIMOTHY S. BATES[5], PHILIP A. DURKEE[6], PETER J. SMITH[6], VOLKER FREUDENTHALER[7], MATTHIAS WIEGNER[7], DAVE S. COVERT[8], SANTIAGO GASSÓ[8], DEAN HEGG[8], DONALD R. COLLINS[9]**, RICHARD C. FLAGAN[9], JOHN H. SEINFELD[9], VITO VITALE[10] and CLAUDIO TOMASI[10], [1]*SRI International, 333 Ravenswood Avenue, Menlo Park, CA;* [2]*Department of Oceanography, University of Hawaii, Honolulu, HI;* [3]*Bay Area Environmental Research Institute, San Francisco, CA;* [4]*NASA Ames Research Center, Moffett Field, CA;* [5]*NOAA-Pacific Marine Environmental Laboratory, Seattle, WA;* [6]*Naval Postgraduate School, Monterey, CA, USA;* [7]*University of Munich, Munich, Germany;* [8]*University of Washington, Seattle, WA;* [9]*California Institute of Technology, Pasadena, CA, USA;* [10]*Istituto FISBAT-CNR, Bologna, Italy*

(Manuscript received 11 February 1999; in final form 4 October 1999)

ABSTRACT

Analyses of aerosol optical depth (AOD) and columnar water vapor (CWV) measurements acquired with NASA Ames Research Center's 6-channel Airborne Tracking Sunphotometer (AATS-6) operated aboard the R/V *Professor Vodyanitskiy* during the 2nd Aerosol Characterization Experiment (ACE-2) are discussed. Data are compared with various in situ and remote measurements for selected cases. The focus is on 10 July, when the Pelican airplane flew within 70 km of the ship near the time of a NOAA-14/AVHRR satellite overpass and AOD measurements with the 14-channel Ames Airborne Tracking Sunphotometer (AATS-14) above the marine boundary layer (MBL) permitted calculation of AOD within the MBL from the AATS-6 measurements. A detailed column closure test is performed for MBL AOD on 10 July by comparing the AATS-6 MBL AODs with corresponding values calculated by combining shipboard particle size distribution measurements with models of hygroscopic growth and radiosonde humidity profiles (plus assumptions on the vertical profile of the dry particle size distribution and composition). Large differences (30–80% in the mid-visible) between measured and reconstructed AODs are obtained, in large part because of the high sensitivity of the closure methodology to hygroscopic growth models, which vary considerably and have not been validated over the necessary range of particle size/composition distributions. The wavelength dependence of AATS-6 AODs is compared with the corresponding dependence of aerosol extinction calculated from shipboard measurements of aerosol size distribution and of total scattering measured by a shipboard integrating nephelometer for several days. Results are highly variable, illustrating further the great difficulty of deriving column values from point measurements. AATS-6 CWV values are shown to agree well with corresponding values derived from radiosonde measurements during 8 soundings on 7 days and also with values calculated from measurements taken on 10 July with the AATS-14 and the University of Washington Passive Humidigraph aboard the Pelican.

* Corresponding author.
e-mail: jlivingston@mail.arc.nasa.gov
** Present affiliation: Texas A&M University, College Station, TX, USA.

1. Introduction

The 2nd Aerosol Characterization Experiment (ACE-2) of the International Global Atmospheric Chemistry Project (IGAC) was conducted from 16 June through 25 July 1997. The goal of ACE-2 was to characterize and understand the properties and controlling factors of the aerosol in the anthropogenically modified atmosphere of the North Atlantic and assess their relevance for radiative forcing (Raes et al., 2000).

During ACE-2, the 6-channel NASA Ames Airborne Tracking Sunphotometer (AATS-6) was operated aboard the Institute of Biology of Southern Seas (Sebastopol, Ukrania) Research Vessel (R/V) *Professor Vodyanitskiy* in the North Atlantic Ocean off the coast of Portugal and North Africa during the period 22 June through 23 July 1997. Measurements were taken in support of the CLEARCOLUMN (Russell and Heintzenberg, 2000) and LAGRANGIAN (Johnson et al., 2000) components of ACE-2.

Since 1985, the AATS-6 has been operated successfully aboard a variety of aircraft platforms and from the ground in several stratospheric and tropospheric research studies (Livingston and Russell, 1989; Pueschel and Livingston, 1990; Russell et al., 1993; Russell et al., 1999a), but the instrument had never been operated from aboard a ship before ACE-2. Shipboard operation of the instrument during transit over the open ocean presented a new set of challenges to the automatic tracking and data acquisition capabilities of the AATS-6 due to platform pitch and roll, radio frequency interference from the ship's radio early in the cruise, intermittent obscuration of the solar disk by shipboard structures and overhanging antenna and support wires, sea salt spray coating of the optical windows that required frequent cleaning, and general operation of the instrument electronics in the corrosive sea salt environment. These problems were mitigated, to a large extent, by conformally coating all electronics within the instrument's telescope head prior to the cruise, by frequent operator monitoring of instrument operation and intervention when necessary during data acquisition, and by careful screening and analysis of the measurements. The result is an archived data set that includes aerosol optical depth (AOD) spectra and associated uncertainties for portions of 13 days of the cruise and measurements of columnar water vapor (CWV) on 10 of these days.

During ACE-2, AATS-6 measurements were taken during a variety of lower tropospheric aerosol loading conditions that included relatively clean air masses that originated over the north Atlantic Ocean and moderately polluted air masses transported from the European continent. In this paper, we show selected AATS-6 AOD and CWV data only and compare these results with corresponding in situ and remote measurements for a small subset of the available measurements. Our primary objective is to investigate MBL AOD closure for the single measurement event that occurred on 10 July 1997, when a variety of simultaneous and near-simultaneous in situ and remote sensing measurements was acquired from ship, aircraft, and satellite. For this case, we compare AODs derived from satellite radiometer (AVHRR) measurements of upscattered radiance with temporally and spatially coincident AATS-6 column AODs, and with AODs measured just prior to satellite overpass within 70 km of the ship by the 14-channel Ames Airborne Tracking Sunphotometer (AATS-14) that operated aboard the Pelican airplane. We calculate MBL AODs at the ship location by subtracting the free tropospheric AODs measured by AATS-14 from the column AODs measured by AATS-6, and these values are compared with MBL AODs estimated from shipboard in situ aerosol size distribution measurements (Quinn et al., 2000; Bates et al., 2000) and from a shipboard aerosol backscatter lidar. We show that demonstration of MBL AOD closure using the shipboard sunphotometer and in situ aerosol size measurements is a complex task that requires a number of critical assumptions.

2. Instrumentation

2.1. 6-Channel NASA Ames Airborne Tracking Sunphotometer (AATS-6)

The AATS-6 (Matsumoto et al., 1987; Russell et al., 1993) tracks the sun and measures the direct beam solar transmission through the earth's atmosphere in 6 spectral channels. Each channel consists of a doubly baffled entrance tube, interference filter, photodiode detector, and integral preamplifier. The entrance baffles define a detector field of

view (FOV) with measured half angle of 2.2°. The 6 filter/detector/preamplifier sets are mounted in a common heat sink maintained at $45° \pm 1°C$. During ACE-2, the filters were centered at wavelengths 380.1, 450.7, 525.3, 863.9, 941.4, and 1020.7 nm, with filter bandwidths (FWHM) of 5.0–5.8 nm. Solar tracking is achieved by azimuth and elevation motors driven by error signals derived from a differential-shadowing sun sensor. Photodiode voltages were digitized at 3 Hz, averaged over 3 s, and recorded every 12 s together with signal standard deviations and various ancillary data.

Calibration of the AATS-6 was performed by taking sunrise measurements at Mauna Loa Observatory on a series of days during late April/early May prior to ACE-2 and again in August following ACE-2. In all channels except 941.4 nm, the Langley plot technique (Russell et al., 1993) was used to derive the exoatmospheric detector voltages that are necessary for subsequent calculation of instantaneous optical depths. At 941.4 nm, because water vapor and aerosol are the primary attenuators and attenuation by water vapor does not follow Beer's Law, a modified Langley technique (Michalsky et al., 1995; Schmid et al., 1996) was used. AODs and associated uncertainties were calculated according to the methodology described in Russell et al. (1993), and CWV estimates and uncertainties were derived using the methodology described in Schmid et al. (1996). Columnar ozone amounts necessary for the calculation of AOD from total optical depth were taken from the Total Ozone Monitor Sensor (TOMS) on the Earth Probe satellite.

AATS-6 measurements acquired during ACE-2 have been filtered to eliminate data affected by clouds by rejecting, for each channel, those points for which the standard deviation of the recorded mean signal voltage exceeded a specified fraction (typically 0.5%) of the mean signal over each 3-s sampling period. Although this screening works quite well in removing large amplitude data excursions that result from solar obscuration (as might be caused by clouds) that lasts for a significant fraction of the 3-s sampling period, it cannot and does not remove shorter-lived or partial obscuration events. One of the major problems associated with shipboard operation of the AATS-6 during ACE-2 was partial or intermittent obscuration of the sun by shipboard structures such as masts and antenna wires. Inclusion of these "contaminated" data in the analysis always results in an overestimate of the calculated optical depth (from 10–100%), can cause an artificial apparent periodic variation in the optical depth temporal traces, and, in general, results in optical depths that are significantly noisier than those calculated during periods when no such interference occurred. The data processing filter described above was unable to remove points like these from the data set, and no attempt has been made to do so, because of the subjectivity required in any such attempt. In particular, one approach to removing these data would be to assume that only the relative minima in calculated optical depth are "uncontaminated", but defining "relative minima" is itself subjective and prone to large uncertainty. The frequency of occurrence of data affected by ship structure obscuration is estimated as less than 10% of the total archived AATS-6 data set. The inclusion of such data in certain figures of this paper is so noted in the text.

2.2. *14-Channel NASA Ames Airborne Tracking Sunphotometer (AATS-14)*

During ACE-2, the AATS-14 was operated on a single engine modified Cessna Skymaster aircraft, the Pelican, which is operated by the Marina, California Center for Interdisciplinary Remotely Piloted Aircraft Studies (CIRPAS). The Pelican flew in and out of the North Airport (28.48°N, 16.34°W, 632 m MSL) on Tenerife, Canary Islands, and included a variety of instruments that measured aerosol chemical, physical, and optical properties, plus radiative fluxes and meteorological parameters. These are summarized by Russell and Heintzenberg (2000). The AATS-14 was designed and developed by NASA Ames, and its first science flights were on the Pelican during the summer 1996 Tropospheric Aerosol and Radiative Forcing Observational Experiment (TARFOX) (Livingston and Russell, 1997; Russell et al., 1999a, 1999b). It measures the transmission of the direct solar beam in 14 spectral channels between 380 and 1558 nm. During ACE-2, the Pelican flew in the vicinity of the R/V *Vodyanitskiy* only during a single flight on 10 July to the northeast of the Canary Islands. Only measurements taken with the AATS-14 on this day are discussed in this

study. Schmid et al. (2000) present in-depth column closure analyses of AATS-14 measurements taken on 8 and 17 July, while Collins et al. (2000) use AATS-14 AODs measured on 21 June, and 8, 10 and 17 July in their study that focuses on the Pelican in situ aerosol measurements. Calibration of the AATS-14 was performed from the ground at Mauna Loa prior to ACE-2 and from aboard the Pelican during several flights near sunset during ACE-2.

2.3. *AVHRR*

The Advanced Very High Resolution Radiometer (AVHRR) is a spaceborne instrument that measures solar radiance backscattered by the earth-atmosphere system in 5 wavelength passbands. In our study, we compare AATS-6 AOD spectra with corresponding AOD spectra derived (Durkee et al., 2000) from AVHRR radiances in channels 1 and 2 (centered at 630 and 860 nm, respectively) during NOAA-14 satellite overpasses on 10 July, 24 and 25 June. Durkee et al. (2000) present an in-depth validation of AODs derived from the AVHRR radiances during ACE-2 by comparing the AVHRR-derived values with corresponding AODs measured by various sunphotometers during satellite overpasses.

2.4. *Shipboard in situ particle sampling instruments*

The NOAA Pacific Marine Environmental Laboratory (PMEL) operated a suite of in situ instruments aboard the R/V *Vodyanitskiy* to measure aerosol size distribution and total and backscattered aerosol light scattering coefficient (at 450, 550 and 700 nm). These instruments and the associated data processing methodology are described in detail by Quinn et al. (2000) and Bates et al. (2000). Aerosol particles were sampled at 10 m above sea level through a heated mast. The instruments included an ultrafine differential mobility particle sizer (UDMPS), a differential mobility particle sizer (DMPS), TSI 3010 and TSI 3025 particle counters, a TSI 3310A aerodynamic particle sizer (APS), and a TSI 3563 integrating nephelometer. The 2 DMPSs and the APS were located within a humidity controlled box at the base of the mast. The sample air flow was maintained at approximately 55% RH to match the sampling RH of the impactors and the integrating nephelometer (Quinn et al., 1998). Particle number-size distributions were collected every 10 min. In this paper, we use the nephelometer total scattering measurements, and the particle number distribution data averaged over 30-min periods centered on the hour and half hour and archived at dry RH of 10% in terms of geometric particle diameter. We adjust the size distributions at 10% RH to ambient RH using either the Swietlicki et al. (2000) ACE-2 ship hygroscopic growth data or the model from Hoppel et al. (1990).

2.5. *Shipboard aerosol backscatter lidar*

The University of Munich Meteorological Institute (LMU) operated its 3-wavelength aerosol backscatter lidar (Wiegner et al., 1995) aboard the R/V *Vodyanitskiy*. The lidar is equipped with a Nd:YAG laser that simultaneously emits radiation at 1064 nm, 532 nm, and 355 nm with pulse energies of 220 mJ, 100 mJ, and 155 mJ, respectively. The receiving telescope with 30 cm diameter has a variable field of view between 0.5 and 8 mrad, and the line of sight of the lidar can be changed in azimuth and zenith direction to observe atmospheric cross-sections or even volumes. During ACE-2, the lidar was operated in a zenith-pointing mode with a field of view between 2 and 8 mrad. Vertical profiles of aerosol backscatter were measured as means over 20 s (200 laser shots) about every 30 min at a sampling rate of 30×10^6 samples/s, which results in a vertical resolution of 5 m at altitudes at least 150–200 m above the lidar. Data below these altitudes are not used due to the incomplete overlap of receiver and transmitter FOV in this region. Measurements acquired with the lidar are used in this study to determine the height of the MBL and to estimate the vertical distribution of aerosols within and above the MBL. For 10 July and 22 July, aerosol extinction coefficients have been derived from the lidar measurements by assuming height-dependent extinction-to-backscatter ratios for different aerosol models according to a parameterization (Ackermann, 1998) with respect to the height-dependent humidity profiles from radiosoundings onboard the vessel.

3. Results

3.1. Overview

As noted by Quinn et al. (2000) and Bates et al. (2000), during ACE-2 the R/V *Vodyanitskiy* encountered air masses from 5 source regions: the central north Atlantic, the Arctic north Atlantic, the Iberian peninsula, the Mediterranean, and western Europe. Fig. 1 shows representative AOD spectra that illustrate the range of AOD values measured by the AATS-6 during flow from the central north Atlantic (22 June), the Mediterranean (6 July), the Iberian peninsula (18 July), and Western Europe (10, 22 July). Mid-visible AODs ranged from a minimum of 0.03 on 22 June to a maximum of 0.35 on 18 July.

AATS-6 AOD and CWV data are available for comparison with measurements by other sensors on several days. Table 1 lists those days for which the highest quality (i.e., fewest number of obscuration events by clouds and/or ship structures) AATS-6 data are available and includes a partial list of available comparative data. In Subsections 3.2 and 3.3, we present detailed case studies of selected AATS-6 AOD measurements acquired on 10 and 22 July, respectively. We also compare AATS-6 CWV values with corresponding values measured by the AATS-14 and by the UWPH on 10 July and derived from radiosonde measurements on 7 days. In Section 4 (summary and conclusions), we compare the spectral behavior of AATS-6 AODs for those days listed in Table 1 with analogous results calculated from shipboard in situ aerosol size distribution and scattering measurements.

We restrict discussion of other AATS-6 measurements to the following brief summary of results from comparative analyses of data acquired on 3 other days. In particular, AVHRR AODs derived from measurements acquired on 24 and 25 June were found to agree with corresponding AATS-6 AODs to within 0.01–0.02. These data are included in Durkee et al. (2000). AATS-6 AOD measurements taken near Sagres on 18 July have been compared with simultaneous measurements taken with the Istituto FISBAT IR-RAD multiwavelength sun-radiometer (Vitale et al., 2000) at the Sagres 50-m site (8°57′W, 36°59′N). Rms differences for data acquired during the period 1000–1700 UTC ranged from 0.015 to 0.021 ($\pm$13% in the mid-visible) in absolute AOD. A similar comparison of CWV values derived from the AATS-6 and Istituto FISBAT ASP-1 sun-photometer measurements (Tomasi et al., 2000) for the same time period on 18 July yielded rms differences of 0.41 g/cm^2 for AATS-6 CWV values of 3.2–3.3 g/cm^2.

The analyses presented in Section 3 focus on

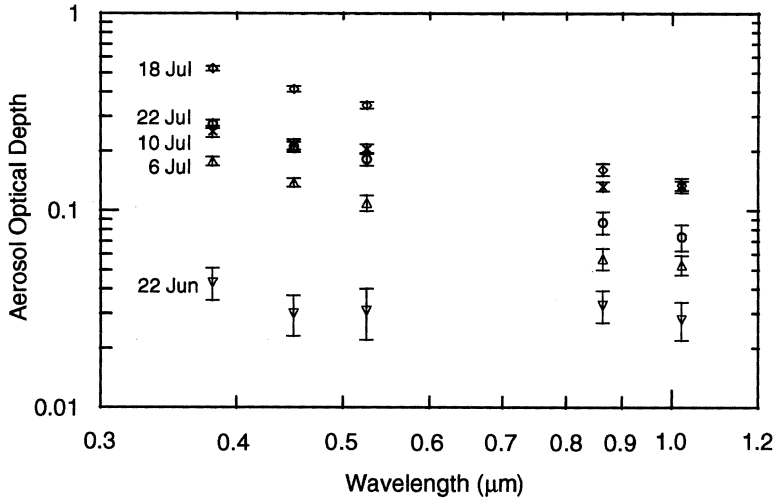

Fig. 1. Representative aerosol optical depth spectra measured by AATS-6 aboard the R/V *Vodyanitskiy* during ACE-2.

Table 1. *Summary of best AATS-6 measurements and partial list of available spatially and temporally near-coincident comparative data*

Date	Air mass classification	AATS-6 (RVV)[1]	AATS-14 (Pelican)	In situ (Pelican)	AVHRR (NOAA-14)	In situ (RVV)	LMU Lidar (RVV)	Radiosonde (RVV) launch time (UTC)	Sagres (50-m site) sunphotometers
22 June	Atlantic	AOD, CWV	—	—	—	asd[2] , tot scat[3]	–	1146, 2244	FISBAT Bologna, Univ. of Leipzig
24 June	Iberian	AOD, CWV	—	—	1445 UTC	asd, tot scat	range-corrected signals	1146, 2246	—
25 June	Iberian	AOD, CWV	—	—	1434 UTC	asd, tot scat	range-corrected signals	1052, 2305	—
27 June	Atlantic/polar	AOD	—	—	—	asd, tot scat	range-corrected signals	1118	—
30 June	polar	AOD	—	—	—	asd, tot scat	range-corrected signals	1047, 2248	—
6 July	Mediterranean	AOD, CWV	—	—	—	asd, tot scat	range-corrected signals	1058, 2302	—
10 July	W. Europe	AOD, CWV	AOD, CWV	Various	1515 UTC	asd, tot scat	relative bks[4]; ext[5]	1657, 2250	—
18 July	Iberian	AOD, CWV	—	—	1524 UTC	asd, tot scat	range-corrected signals	1058, 1650	FISBAT Bologna, Univ. of Leipzig
22 July	W. Europe	AOD, CWV	—	—	—	tot scat	relative bks; ext	1046, 1654, 2246	—

[1] RVV: R/V *Vodyanitskiy*.
[2] asd: aerosol size distribution measured by particle samplers/sizer.
[3] tot scat: aerosol total scattering coefficient measured by integrating nephelometer.
[4] bks: aerosol backscatter.
[5] ext: aerosol extinction.

data collected on 10 July, when nearby AATS-14 measurements aboard the Pelican provided a measure of AOD above the MBL and permitted calculation of MBL AOD from the shipboard AATS-6 measurements of total column AOD at the time of an AVHRR overpass. For this day, aerosol extinction profiles are calculated for a range of refractive indices from the shipboard particle size distribution measurements by using radiosonde RH profiles as input to a hygroscopic growth model. These profiles are then compared with analogous profiles inferred from the LMU lidar backscatter measurements, and they are integrated within the MBL to yield estimates of AOD that are then compared with AATS-6 MBL AODs. Comparisons of AATS-6 and AATS-14 AODs with corresponding values derived from the AVHRR radiance measurements are also shown. For 22 July, AATS-6 AODs are compared with corresponding AODs calculated from simultaneous lidar backscatter measurements.

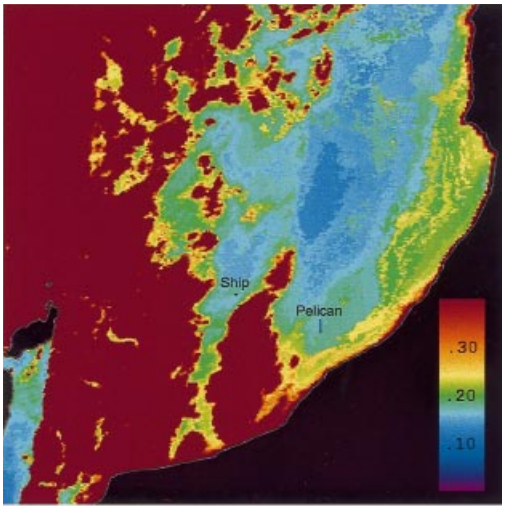

Fig. 2. Aerosol optical depth ($\lambda = 630$ nm) retrieved from AVHRR radiances (Durkee et al., 2000) during 1515 UTC NOAA-14 overpass of the ACE-2 sampling region on 10 July 1997; locations of R/V *Vodyanitskiy* during the period 1451–1524 UTC and Pelican during the period 1454–1500 UTC.

3.2. 10 July 1997

3.2.1. Air mass origin. 5-day backward trajectories calculated by the Royal Dutch Meteorological Institute (KNMI; Scheele et al., 1996) for the ship location ($\sim$29.2°N, 11.7°W) at 1200 UTC on 10 July indicate that the MBL was dominated by flow from western Europe. In particular, air parcels arriving at 975 hPa at the ship location originated over Great Britain at 814 hPa, followed a southward trajectory over France, west over the northern coast of Spain, and finally south over the ocean just west of the Iberian peninsula. Air parcels arriving at the ship location at 850 hPa and above originated 5 days earlier over the north central Atlantic and followed a strictly marine trajectory. All trajectories showed subsidence.

3.2.2. Comparison of AATS-6, AATS-14 and AVHRR column AODs. AATS-6 measurements of AOD can be compared with corresponding AODs that have been derived (Durkee et al., 2000) from AVHRR radiance measurements acquired during a NOAA-14 satellite overpass at 1515 UTC. Measurements of AOD above the Pelican were acquired with the AATS-14 at altitudes 55–70 m MSL in a region approximately 70 km ESE of the ship just prior to the AVHRR overflight. Fig. 2 presents a color coded map of AVHRR AOD calculated from measurements in the 630-nm AVHRR channel, and shows the locations of the ship at 1515 UTC and the airplane during its low altitude traverse between 1457 and 1500 UTC. Note that AVHRR AODs are similar at the ship and Pelican locations. (In fact, as shown in Figs. 3b, c below, values at the 2 locations in AVHRR channel 2 were equal, and those in AVHRR channel 1 were within 0.01.) Fig. 3a shows the temporal variation of AOD measured by AATS-6 during the period 1451–1524 UTC. Relative maxima in AOD were measured from 1454 to 1457 UTC, or about 20 min prior to satellite overpass, with mid-visible values near 0.20. Relative minima were measured from 1509 to 1513 UTC, with mid-visible values about 0.15. Values at 1515 UTC were about 0.01 greater. The magnitude of the difference between mean AOD values measured in the relative maxima and minima was about 0.05 at all wavelengths, and this near wavelength-independent variation in AOD strongly suggests that attenuation by large particles — perhaps thin clouds — may have been the source of the larger AOD values. However, there is no evidence of cirrus or lower level clouds in the simultaneous lidar backscatter profiles at 1064 nm, so the attenuating aerosol particles must

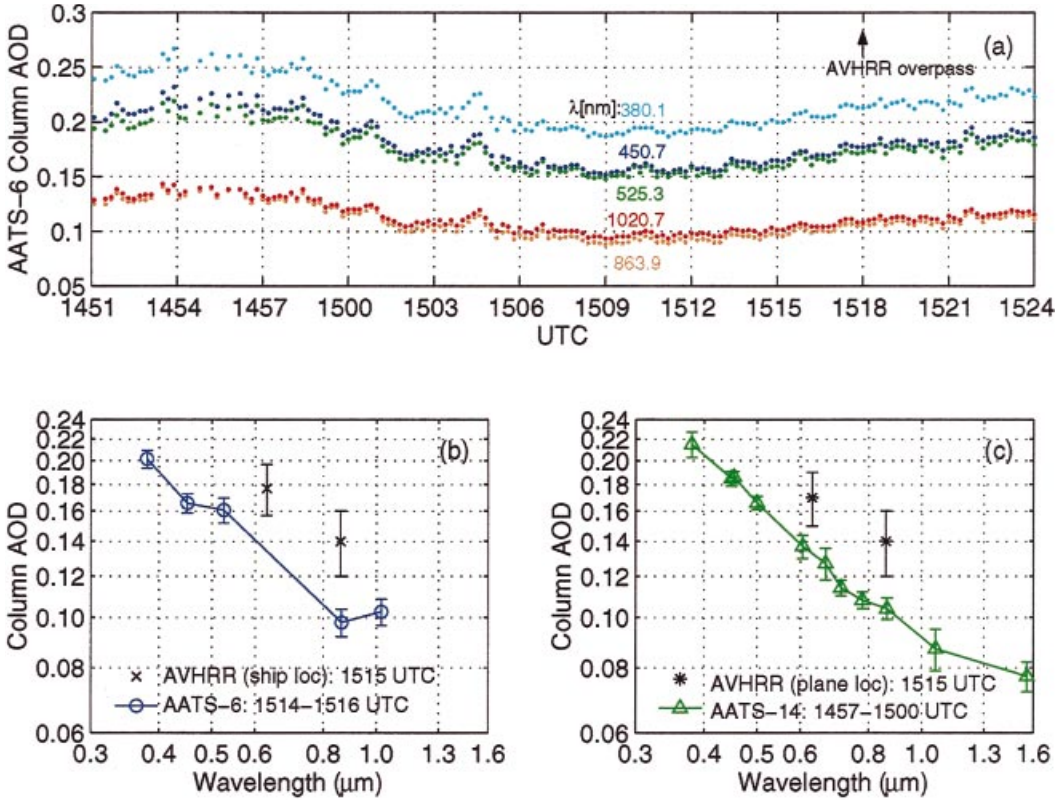

Fig. 3. For 10 July 1997: (a) temporal variation of total column aerosol optical depth measured by AATS-6 aboard the R/V *Vodyanitskiy*, (b) comparison of AATS-6 aerosol optical depths and AVHRR aerosol optical depths calculated for the ship location, (c) comparison of AATS-14 aerosol optical depths acquired from the Pelican at an altitude of 60 m ASL and AVHRR aerosol optical depths calculated for the plane location.

have been within the layer between the sea surface and ~150 m MSL, where no useful LMU lidar backscatter data have been retrieved.

Fig. 3b compares a 2-min mean AOD spectrum measured by AATS-6 during the time of the AVHRR overflight with AODs calculated in the 2 AVHRR channels for the ship location. Vertical bars on the AATS-6 AODs represent mean measurement uncertainties (including calibration, gas optical depth, etc. per eq. (A22a) of Russell et al., 1993); they are slightly greater than the sample standard deviations during the averaging period. Vertical bars on AVHRR AODs represent the uncertainty based solely on the radiometric resolution of the satellite and do not include any uncertainty associated with the retrieval algorithm (Durkee et al., 2000). AVHRR AODs exceeded the AATS-6 values by about 0.04, which is more than the estimated uncertainties. The source of this difference has not been identified. Fig. 3c compares AOD measurements acquired with the AATS-14 during the Pelican's low altitude traverse 15 min before the AVHRR overpass with AVHRR AODs calculated for the Pelican location. AVHRR values also exceeded mean AATS-14 AODs by about 0.04, but AATS-14 values do not include the AOD in the layer between the sea surface and the altitude of the Pelican. Fig. 4 shows vertical profiles of AOD measured by the AATS-14 during aircraft ascent from 70 m to 3.8 km during the period 1500–1605 UTC, and the corresponding retrieved aerosol extinction profiles (see Schmid et al. (2000), for details of the retrieval algorithm). It is estimated by summing extrapolated values of the retrieved aerosol extinction shown in Fig. 4 down to the sea surface that about 0.010–0.015

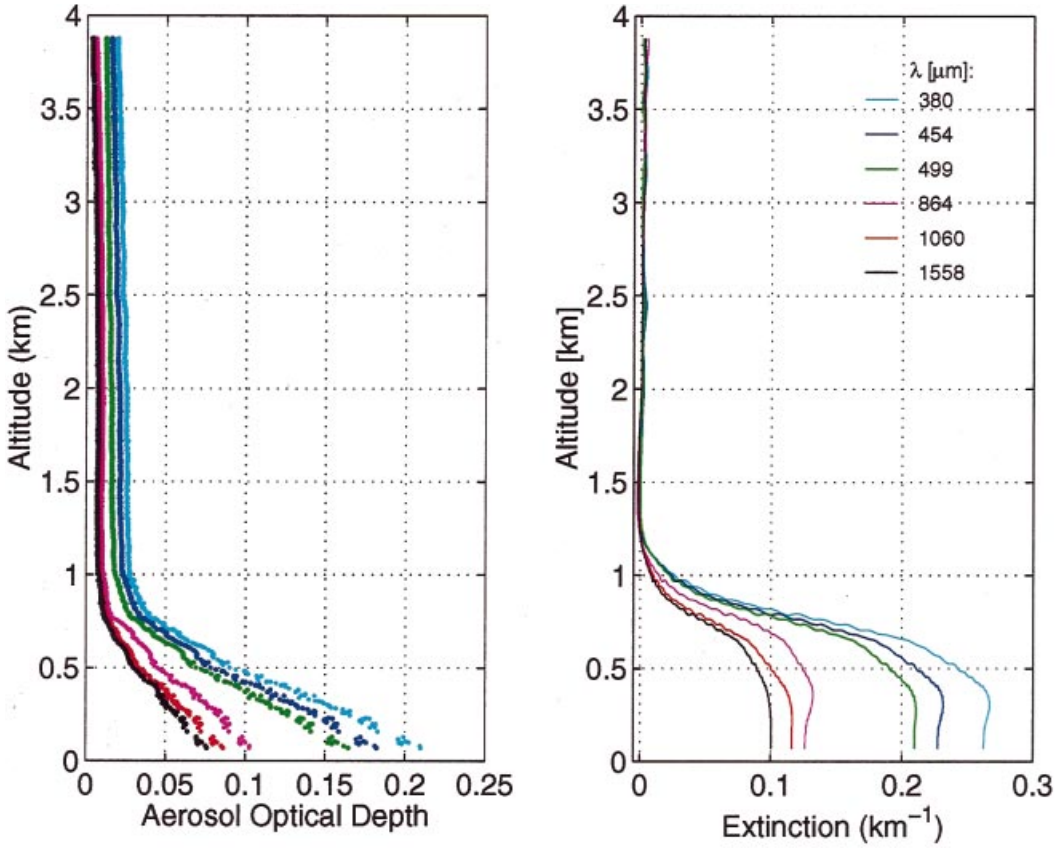

Fig. 4. Aerosol optical depth and extinction profiles retrieved from AATS-14 measurements made between 1500 and 1515 UTC during Pelican flight near R/V *Vodyanitskiy* on 10 July 1997.

(depending on wavelength) of the 0.04 difference between AVHRR and AATS-14 AOD can be explained by the AOD in the layer between the sea surface and the Pelican. The remainder of the difference is attributed to temporal variation in AOD between the time of the AATS-14 low altitude measurements and the AVHRR overpass time.

3.2.3. Columnar water vapor measurements. Fig. 5 compares values of CWV and water vapor density derived from AATS-14 measurements taken in the 940-nm channel (see Schmid et al. (2000), for details of the retrieval algorithm) during aircraft ascent with corresponding values derived from coincident measurements taken aboard the Pelican with the University of Washington Passive Humidigraph (UWPH) (Gassó et al., 2000) and with values calculated from the 1657 UTC ship radiosonde measurements. The mean CWV value derived from shipboard measurements taken in the AATS-6 941.4-nm channel during the 1500–1730 UTC time period is also shown in Fig. 5. Horizontal bars on the AATS-14 and AATS-6 CWV values represent the uncertainty in the measurements and are due primarily to the uncertainties in the calibration voltages in the respective water vapor channels. Derivation of these uncertainties is described in detail by Schmid et al. (1996). The AATS-6 CWV mean value slightly underestimates corresponding values derived from the AATS-14, the UWPH, or the radiosonde, but values agree to within measurement uncertainties. Fig. 6 compares CWV values calculated from AATS-6 measurements with corresponding values derived from 8 radiosonde measurements for 7 days during ACE-2. Values

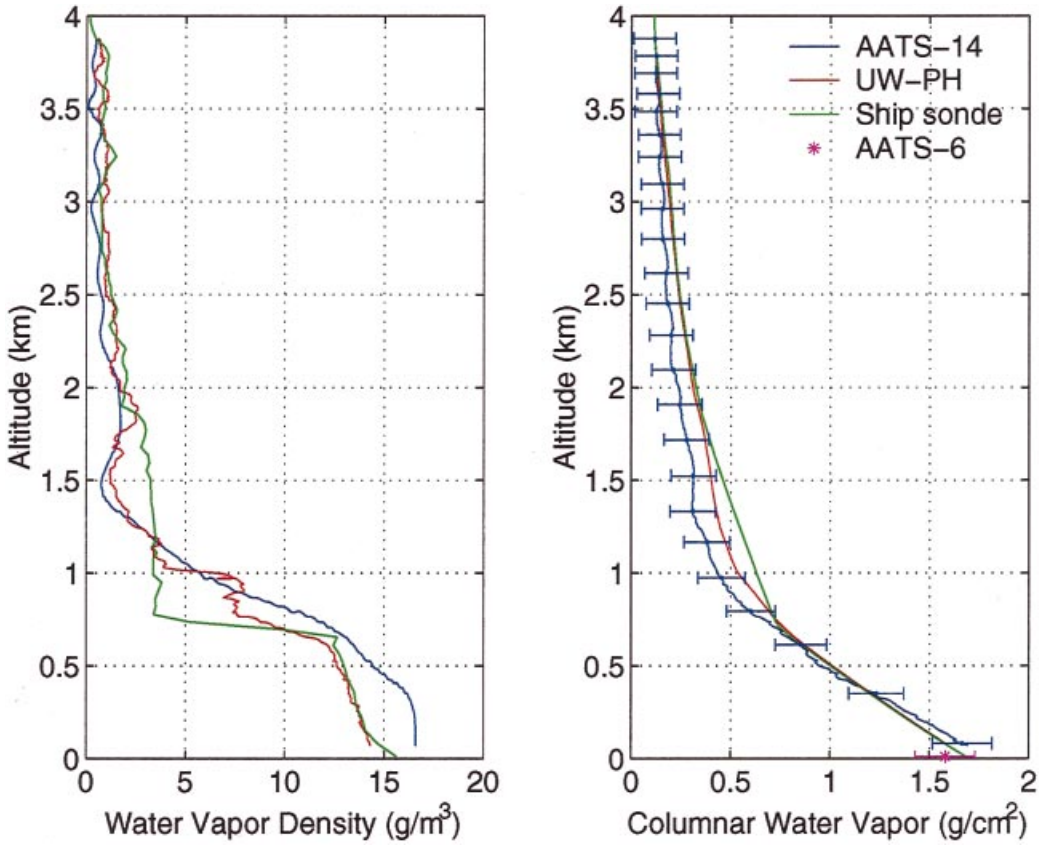

Fig. 5. For 10 July 1997: water vapor density and columnar water vapor profiles calculated from AATS-14 measurements and from UWPH measurements (Gassó et al., 2000) during Pelican ascent 1500–1605 UTC, and from ship radiosonde 1656–1715 UTC; mean columnar water vapor retrieved from AATS-6 measurements 1500–1730 UTC.

agree well, with an rms difference of 0.10 g cm^{-2} for a range of 1.2 to 3.2 g cm^{-2}.

3.2.4. MBL aerosol extinction and optical depth. At the ship location, AODs have been calculated within the MBL by subtracting from the AATS-6 total column AOD values the free-tropospheric AODs measured by the AATS-14 in the altitude range 1.09–1.17 km (cf. Fig. 4), which was just above the top of the MBL at the Pelican location. As will be shown below, the top of the MBL at the Pelican location was about 0.3 km higher than that measured at the ship location by lidar at 1513 UTC. The free-tropospheric AODs ranged from 0.027 at 380.1 nm to 0.008 at 1020.7 nm. The resulting AATS-6 MBL AODs will be compared with corresponding values calculated from coincident shipboard mean in situ measurements of aerosol size distribution combined with an assumption on the vertical mixing behavior (e.g., uniform mixing) within the MBL.

3.2.4.1. Hygroscopic growth. First, the in situ aerosol size distribution must be adjusted for hygroscopic growth. Two separate hygroscopic growth models were used together with the RH profile measured by ship radiosonde at 1700 UTC. The first model is that of Swietlicki et al. (2000), in which

$$D_{\mathrm{p}}(\mathrm{RH}) = D_{\mathrm{p10}}\, 10^{c}(1 - \mathrm{RH}/100)^{\gamma}, \qquad (1)$$

where $D_{\mathrm{p}}(\mathrm{RH})$ is the particle diameter at RH; D_{p10} is the particle diameter at 10% RH; and c and γ are parameters derived from H-TDMA measurements taken aboard the R/V *Vodyanitskiy* during ACE-2 European outbreak air masses for a range

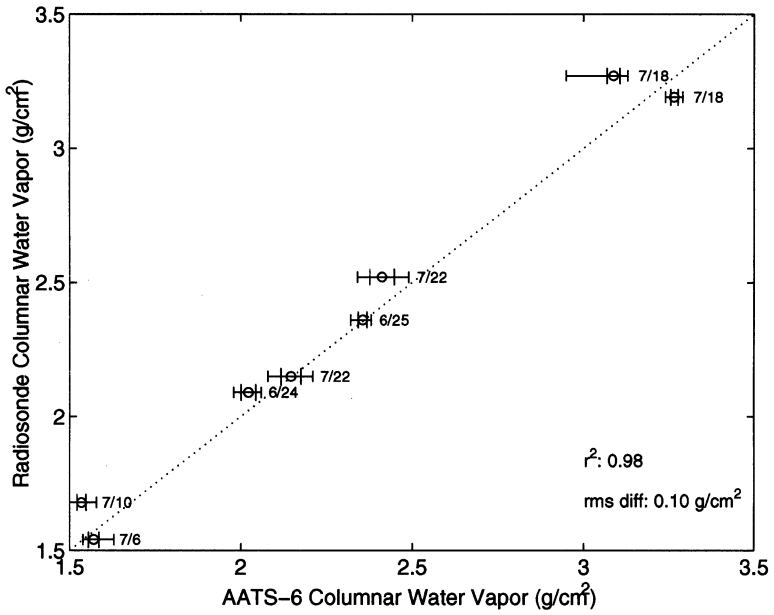

Fig. 6. Scatter diagram of columnar water vapor calculated from radiosonde measurements and from AATS-6 measurements during ACE-2. Each AATS-6 data point represents the mean calculated over the time period spanned by the radiosonde measurements; horizontal bars show the corresponding standard deviation (wide ticks) and the range (narrow ticks) for that time period.

of particle sizes (50–250 nm dry particle diameter) within the Aitken and accumulation modes. Although the actual measurements do not extend beyond 250 nm diameter, we have applied the Swietlicki et al. (2000) model to all particles with dry (10% RH) diameters $\leqslant 1.2$ μm. This represents an extrapolation of the actual measurements. For particles with dry diameters > 1.2 μm, we have used an analogous growth curve based on the Swietlicki et al. (2000) measurements for sea spray particles at Punta del Hidalgo, Tenerife during incidents of local pollution. We shall refer to this composite model as the S model. The second model is that of Hoppel et al. (1990), in which separate growth curves are presented for particles with dry diameters < 1 μm and for sea spray aerosol particles with diameters > 3 μm. The Hoppel et al. sea spray curve is taken from Hänel (1976). Following the procedure used by Hoppel, we interpolated between the 2 Hoppel et al. model curves for intermediate particle sizes. We shall refer to this model as the H model. Fig. 7a shows the 1500 UTC aerosol size distribution dried to 10% RH and resultant humidified size distributions after application of the S hygroscopic growth model for relative humidities of 80% and 90%. Fig. 7b shows the analogous results after application of the H model.

Figs. 7c, d present the corresponding particulate extinction spectra calculated from the in situ aerosol size distribution measurements for 3 refractive indices: $1.33 - 0i$ (similar to pure water), $1.40 - 0.0035i$ (tropospheric aerosol model: Tanré et al., 1997), and 1.48–0.01i (polluted continental aerosol). Calculations using the *S* and *H* particle growth models give similar results, with the expected strong dependence of extinction on RH due to change in particle size, and a weaker dependence on refractive index. Model-to-model extinction differences (*S*–*H*) vary from +6% (380 nm) to −11% (1020 nm) for RH 80%, and +12% (380 nm) to +1% (1020 nm) for RH 90%.

Table 2 presents percent mass fractions calculated from the shipboard 7-stage Berner impactor sample collected during the period 0650 UTC on 10 July to 0600 UTC on 11 July. For stage 4, for which the dry particle geometric cutoff diameter is about 0.67 μm (which corresponds to a 55%

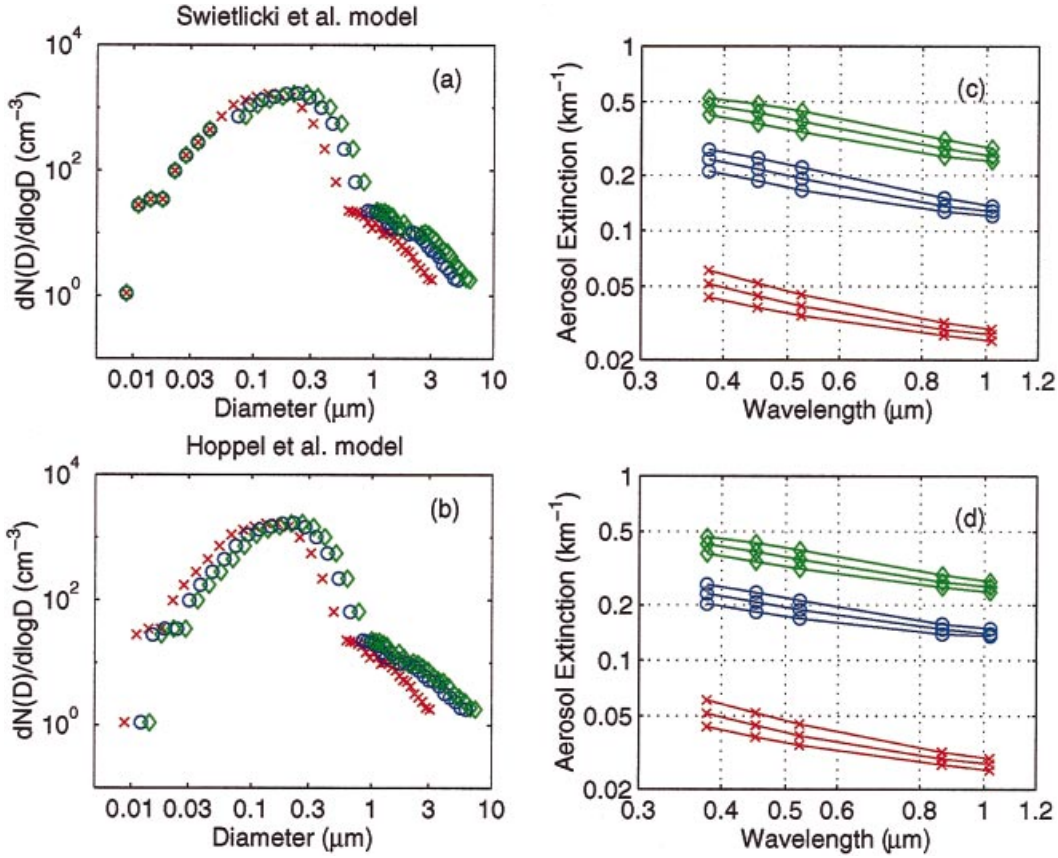

Fig. 7. NOAA/PMEL aerosol size distribution measured aboard R/V *Vodyanitskiy* at 1500 UTC on 10 July 1997 (a, b); corresponding calculated extinction spectra (c, d). Dried (RH = 10%: × symbols) size distribution has been humidified to 80% (circles) and 90% (diamonds) RH using hygroscopic growth models of (a) Swietlicki et al. (2000), and (b) Hoppel et al. (1990). Corresponding particulate extinction spectra calculated at AATS-6 wavelengths for 3 refractive indices: $m = 1.33 - 0i$ (smallest values for each set of 3), $m = 1.40 - 0.0035i$ (intermediate values for each set of 3), and $m = 1.48 - 0.01i$ (largest values for each set of 3).

Table 2. *Percent mass fractions calculated from measurements taken aboard the R/V* Vodyanitskiy *with the NOAA/PMEL 7-stage Berner impactor during the period 0650 UTC 10 July to 0600 UTC 11 July 1997; data are shown for each stage of the impactor*

Impactor stage:	1	2	3	4	5	6	7
D, aero (μm)	0.184	0.308	0.549	1.063	2.024	4.13	10.3
$D_{RH:55\%}$, geom (μm)	0.14	0.24	0.42	0.81	1.55	3.1	7.9
$D_{RH:80\%}$, geom (μm)		0.35	0.61	1.18	2.26	4.53	11.54
nssSO_4	45.93	69.30	70.24	62.45	9.29	2.53	2.08
sea salt	5.00	2.03	3.18	18.59	75.36	86.08	81.92
NO_3	0.00	0.00	0.00	0.00	11.10	9.67	11.24
MSA	0.00	0.48	0.77	0.62	0.13	0.00	0.00
NH_4	6.56	13.65	21.47	13.22	0.00	0.00	0.00
total carbon	42.51	14.54	4.33	5.11	4.12	1.71	4.77

RH particle diameter of about 0.81 μm), 18.6% of the mass was sea salt and 62.4% was non-seasalt sulfate. For stage 5, for which the dry particle geometric diameter is about 1.3 μm, 75% of the mass was sea salt, 9% was non-seasalt sulfate, and 11% was ammonium. Using chemical composition measurements made on Tenerife, Collins et al. (2000) have constructed a model of the size-segregated chemical composition of the boundary layer aerosol for this day. For a particle diameter of 1.0 μm, their results indicate that about 75% of the mass was sea salt. Hence, our assumption that all particles >1.2 μm were sea salt is not entirely correct. This probably leads to a small overestimate of aerosol extinction, because the 90% RH Swietlicki et al. growth factor for sea salt exceeds the corresponding non-sea salt growth factor by about 23%. We note further that our extinction calculations make the unrealistic assumption that refractive index is independent of particle size and wavelength. Clearly, the variation in chemical composition and associated variation in refractive index should be taken into account, but Tang (1996) concluded that the chemical effect on light scattering was outweighed by the size effect for the range of aerosol systems that he considered, which included various ammonium, sodium, sulfate, and nitrate species.

3.2.4.2. Aerosol extinction profile comparison. A spectral aerosol extinction profile can be inferred from the measured shipboard particle size distribution by combining the measured radiosonde RH profile with an assumed vertical distribution of particle number concentration. Using the 1657 UTC radiosonde sounding in an approach similar to that of Hoppel et al. (1990), we have assumed that particle number concentration remained constant up to the height of the maximum in RH (which Hoppel defined as the top of the mixed layer), and then decreased linearly with altitude to a value equal to 50% of the surface value up to the top of the MBL. There is some question as to the heights of the mixed layer and the MBL. NOAA/PMEL analysis (Johnson et al., 1993) of the radiosonde data defines the top of the mixed layer as the altitude where the relative humidity stops increasing with altitude, and the top of the boundary layer as the altitude where the temperature inversion starts and the RH begins to decrease with increasing altitude. This definition is similar, but not identical, to the Johnson et al. (2000) definition of the surface mixed layer (SML). The SML is defined as the layer closest to the surface and is identified by constant equivalent potential temperature with a top defined by the lowest height where the RH stops increasing with height. Johnson et al. (2000) note that RH also increases again in the cloud layer (CL), which is the layer (above the SML) in which clouds form and is also characterized by a nearly equal but smaller equivalent potential temperature. The temperature and RH profiles measured by the ship radiosonde at about 1100 and 1700 UTC and the RH profile measured by the Pelican during its ascent 1500–1515 UTC are shown in Fig. 8a. The NOAA analysis gives a mixed layer height of 570 m and a boundary layer height of 620 m for the 1657 UTC sounding, which measured a near surface RH of 83%, a peak of 91% between 570 and 610 m, and a decrease to 30% at 730 m. A subsidence temperature inversion extended from 610 to 810 m.

Background range-corrected lidar backscatter profiles measured at 532 nm by the LMU shipboard lidar are overplotted in Fig. 8b for 7 times from 1414 UTC to 1726 UTC. The lidar relative backscatter profile measured at 1513 UTC indicates an aerosol layer with a peak backscatter return at about 670 m, and a rapid signal decrease over the next 100 m in altitude. As can be seen in Fig. 8c, the peak of this maximum lidar backscatter signal generally decreased in altitude with time. At 1700 UTC, although the maximum backscatter signal was measured at 470 m, the peak was broad with no significant decrease in backscatter signals up to 620 m, which is consistent with the radiosonde measured height of the maximum RH. The 499-nm aerosol extinction profile (Fig. 4) derived from the AATS-14 optical depth measurements during the period 1500–1515 UTC indicated a broad peak in extinction of 0.21 km^{-1} up to about 350 m, a linear decrease to 0.16 km^{-1} at about 640 m, and a less steep decrease to about 0.05 km^{-1} at 0.9 km, with free tropospheric values (<0.01 km^{-1}) above 1.2 km. In the discussion that follows, we use a value of 610 m for the height of the well-mixed layer and a value of 780 m for the height of the MBL.

Fig. 9 shows plots of aerosol extinction profiles calculated for a refractive index of $1.40 - 0.0035i$ from the 30-min average shipboard aerosol size distribution measurements at a wavelength of

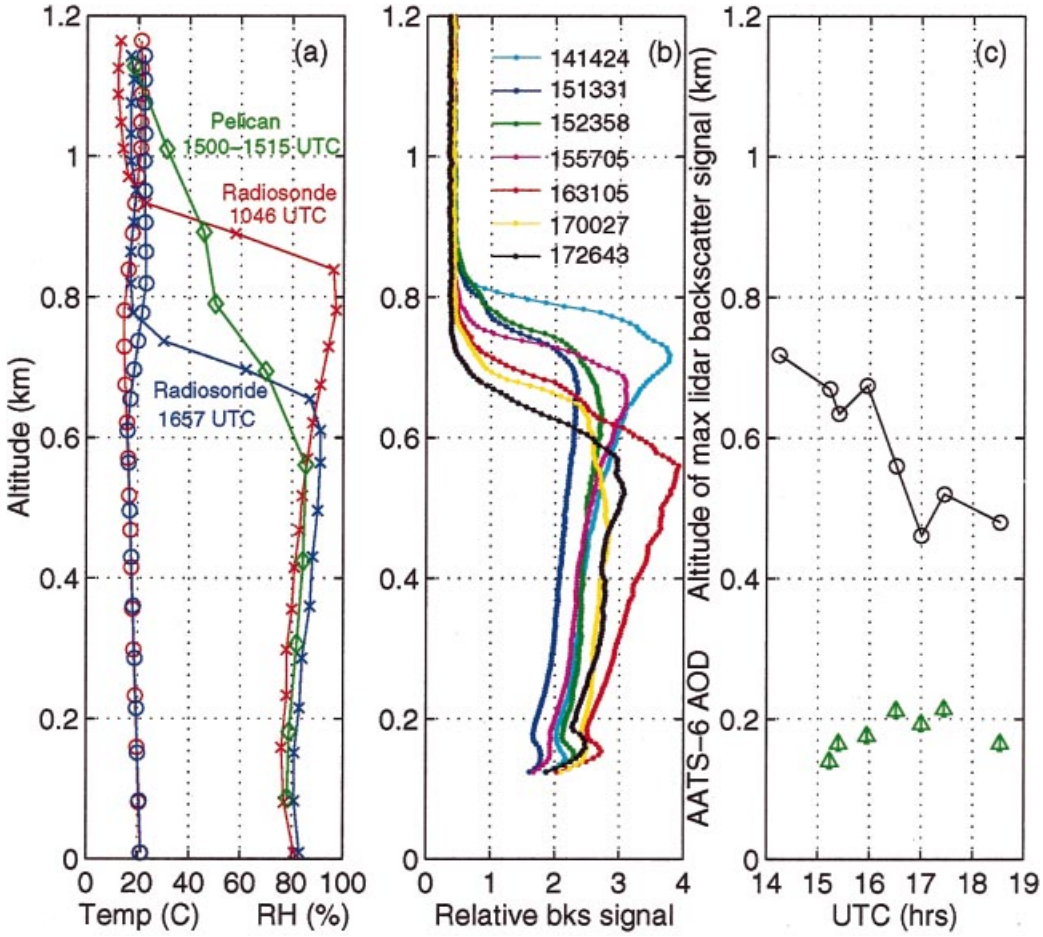

Fig. 8. For 10 July 1997: (a) ship radiosonde temperature and RH profiles, Pelican RH profile; (b) shipboard lidar (University of Munich) relative backscatter profiles at 532 nm between 1414 and 1726 UTC; and (c) time variation of the height of aerosol lidar backscatter signal peak and AATS-6 marine boundary layer aerosol optical depth at 525 nm.

525 nm for 1500 UTC (Fig. 9a) and at all 5 AATS-6 wavelengths for 1700 UTC (Fig. 9b). The 1657 UTC radiosonde RH values are listed at each height. Also plotted in Fig. 9a is the corresponding extinction profile calculated when the Pelican RH profile is used with the ship aerosol measurements. Fig. 9c compares the 525-nm extinction profile shown in Fig. 9a with a profile derived from the AATS-14 airborne optical depth measurements in the 499.4-nm channel (data in the 524.7-nm channel were not usable during this flight due to dirt on the channel aperture window), a profile calculated at 525 nm by Collins et al. (2000) from airborne (Pelican) in situ size distribution and RH measurements, and 2 profiles derived at 532 nm from the shipboard lidar backscatter measurements. The lidar extinction profile was derived from the lidar backscatter measurements using the Ackermann (1998) formulation of an extinction to backscatter model representative of a continental aerosol. This extinction to backscatter model is height dependent in that it varies with RH. The range of RH values (83–91%) measured in the mixing layer by the 1657 UTC sounding results in model extinction to backscatter ratios of 65–72 sr. The shape of the aerosol extinc-

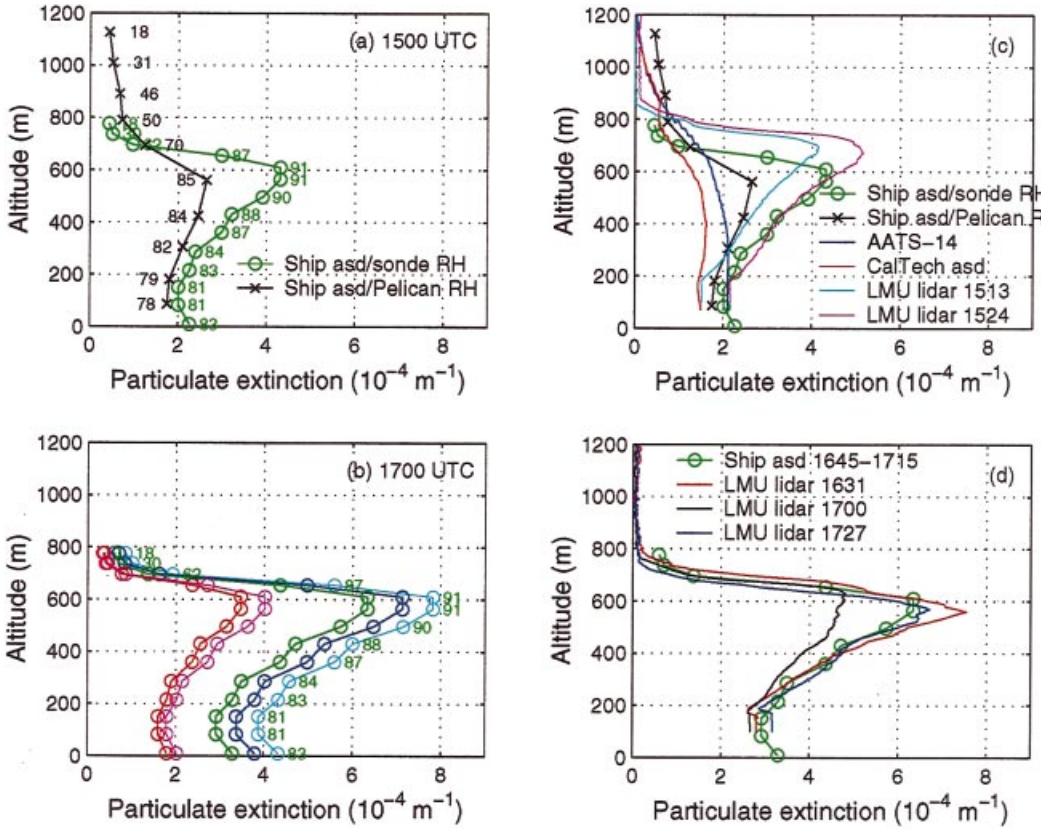

Fig. 9. For 10 July 1997: (a) profiles of aerosol extinction calculated at 525 nm for a refractive index of $1.40 - 0.0035i$ by combining shipboard mean aerosol size distribution measurements during the period 1445–1515 UTC with the radiosonde RH profile measured 1656–1715 UTC above ship location and with the RH profile measured by Pelican UWPH (Gassó et al., 2000) during aircraft ascent 1500–1605 UTC; RH values are listed beside the data points. (b) Aerosol extinction profiles calculated at 5 AATS-6 wavelengths by combining shipboard 30-min average particle size distribution measurements centered at 1700 UTC and 1700 UTC radiosonde RH profile. (c) Comparison of mid-visible aerosol extinction profiles calculated from ship (1445–1515 UTC) and from aircraft (1500–1515 UTC; Collins et al., 2000) in situ particle size distribution measurements, from AATS-14 measurements (1500–1515 UTC), and from shipboard lidar backscatter measurements for times near 1500 UTC. (d) Comparison of mid-visible aerosol extinction profiles calculated from shipboard in situ aerosol size distribution measurements and from shipboard lidar backscatter measurements for times near 1700 UTC.

tion profile calculated from the shipboard in situ size distribution data is tied directly to the shape of the 1700 UTC radiosonde RH profile through the hygroscopic growth model. It differs markedly from the shape of the extinction profile derived from the AATS-14 measurements, and its extinction magnitudes significantly exceed the corresponding AATS-14 values. The shapes of the lidar extinction profiles at 1513 and 1524 UTC are similar to that of the shipboard in situ extinction profile. However, the corresponding peaks in extinction occur at greater altitudes, and indicate that the height of the mixed layer was, in fact, greater at 1500 UTC than at the time of the sounding at 1700 UTC. This is confirmed in Fig. 9d, where lidar profiles measured near 1700 UTC peak at altitudes near the RH peak measured by the radiosonde. Also, the radiosonde RH maximum decreased with time, as shown in Fig. 8. Lidar extinction values at altitudes between 300 and 800 m significantly exceed the AATS-14 values. The shape of the Collins et al. profile

(labeled CalTech), which is derived from in situ measurements in the Pelican profile, is similar to that of the AATS-14 profile, and the values slightly underestimate the AATS-14 extinction (cf. Collins et al., 2000).

There are a number of possible explanations for the large differences in magnitude and in shape between the aerosol extinction profiles calculated from the shipboard measurements and the corresponding profiles derived from the airborne measurements. First, although nearly coincident in time, the shipboard and airborne measurements were separated by 70 km. Thus, it is likely that the instruments did, in fact, sample air masses with slightly different vertical distributions of aerosol. Second, because the above analyses (except Collins et al. (2000)) assume that particle number concentration is constant within the well-mixed layer, our methodology for calculating extinction from the ship in situ measurements is critically dependent on the RH profile. This means that any overestimate in the true RH profile due to a lack of available coincident data, such as occurred at 1500 UTC, or due to inherent uncertainty in the RH measurement can lead to large overestimates in extinction. The RH profile measured at the Pelican location during aircraft ascent 1500–1515 UTC differed significantly from that measured by the 1700 UTC ship sounding (c.f. Fig. 8a). Use of these Pelican RH measurements to adjust the ship in situ measurements of aerosol size distribution for hygroscopic growth yields a profile with values that are significantly closer in magnitude to those of the aircraft sensor profiles. Third, we assume that all particles regardless of size are equally mixed within the mixing layer, and this can lead to an overestimate of extinction and AOD because it does not account for sedimentation of large particles. Fourth, because the hygroscopic growth model for sea salt particles with dry diameters >1.2 μm yields growth factors that exceed those for the smaller particles in the Aitken and accumulation size modes, our application of the sea salt growth curve to all particles >1.2 μm likely leads to a small overestimate in extinction, since all particles >1.2 μm were not sea salt. However, this effect is not enough to account for the differences in magnitude between the extinction profile calculated from the ship in situ aerosol size distribution measurements and that derived from the aircraft measurements. Finally, we acknowledge that our assumption of a particle size- and wavelength-invariant refractive index ($1.40-0.0035i$) is an oversimplification. Nevertheless, the extinction values in Figs. 7c, d, calculated for a range of refractive indices ($1.33-0i$, $1.40-0.0035i$, $1.48-0.01i$), suggest that reasonable variations in refractive index (caused, e.g., by water uptake) would change extinction by less than the size effects explored here.

3.2.4.3. Aerosol optical depth comparison. Fig. 10 compares temporally averaged AATS-6 MBL AOD spectra and corresponding AOD spectra derived by integrating to 780 m the extinction profiles calculated (at the 3 values of refractive index) from the 30-min average shipboard in situ aerosol size distribution measurements centered at 1500 and 1700 UTC. For the range of refractive indices assumed, when non sea-salt growth factors are applied to all particles $\leqslant 1.2$ μm and sea salt growth factors are applied to all particles >1.2 μm prior to calculating extinction, the in situ values significantly overestimate the sunphotometer optical depths for both times. These results are shown by the solid red, green, and blue lines. For a refractive index of $1.40-0.0035i$, the calculated mid-visible AOD exceeds the AATS-6 measurement by about 0.03 (15%) at 1500 UTC, and by about 0.10 (40%) at 1700 UTC. However, use of only the non-sea salt Aitken and accumulation mode growth curves for particles of all sizes (red, green, and blue dashed lines) leads to agreement, within the AOD measurement uncertainties, between measured and calculated AOD for this refractive index at 1500 UTC, but does not completely account for the disagreement at 1700 UTC. Lowering the maximum altitude limit of integration (not shown) to 610 m for the 1700 UTC case (consistent with both lidar and radiosonde) further reduces AODs by about 0.05, which is still 0.03 greater than the mean AATS-6 mid-visible AOD but only about 0.015 greater than the upper limit measurement uncertainty. It should be noted that the AATS-6 mean for 1500 UTC is only a 20-min average, because data before 1450 UTC were affected by ship structure obscuration of the sun. Vertical bars on the AATS-6 values represent the larger of the standard deviation over the time period and the measurement uncertainty. As discussed above and shown in Fig. 3, total column AODs decreased by about 0.05 at all wavelengths during the 1450–1510 UTC time period.

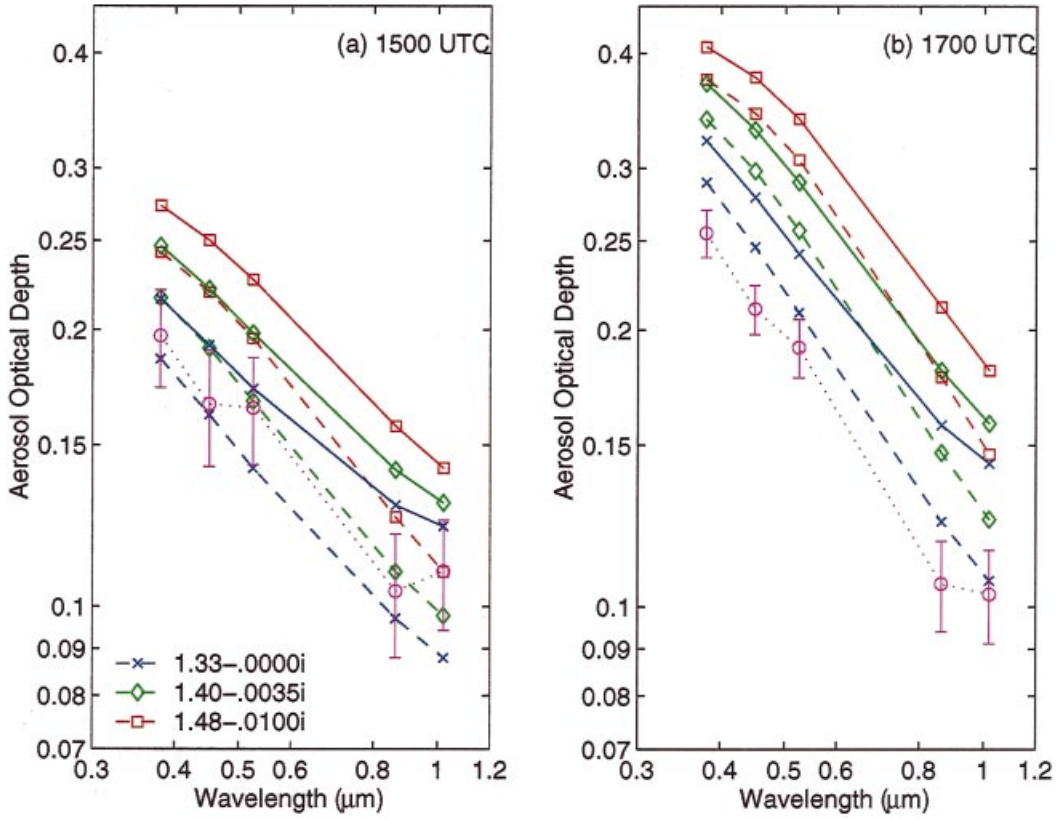

Fig. 10. For 10 July 1997: marine boundary layer aerosol optical depth spectra derived from AATS-6 measurements (circles with error bars) and calculated from shipboard in situ aerosol size distribution measurements for 3 values of refractive index for (a) 1500 UTC and (b) 1700 UTC. For in situ results connected by dashed red, green, and blue lines, growth factors based only on the Swietlicki et al (2000) shipboard measurements for non-sea salt Aitken and accumulation modes were used. For the results connected by solid red, green, and blue lines, the non-sea salt growth factors were used for particles with dry diameter <1.2 μm, and growth factors based on the Swietlicki et al. (2000) sea salt measurements were applied to particles with dry diameter $\geqslant 1.2$ μm.

The time history of AATS-6 AOD and CWV is shown in Fig. 11a for the time period 1400–1830 UTC. Fig. 11b shows corresponding values computed by integrating to 780 m the particulate extinction profiles calculated from the shipboard aerosol size distribution measurements for a refractive index of $1.40 - 0.0035i$ after applying the S hygroscopic growth model as described above, using the 1657 UTC RH profile. In general, mid-visible AODs calculated from the shipboard in situ particle size measurements overestimate coincident AATS-6 AODs by 0.02 to 0.10.

3.2.4.4. Spectral dependence of AOD, extinction, scattering. The wavelength dependence of aerosol optical depth, extinction (E), or scattering (s) is often approximated by a power law,

$$p(\lambda) = p(\lambda_0)\left(\frac{\lambda}{\lambda_0}\right)^{-\alpha}, \tag{2}$$

where the Mie scattering parameter p is AOD, E, or s; λ is wavelength; α represents Ångström exponents, α_D, α_E, or α_s, that can be derived from linear least squares fits to the AOD(λ), $E(\lambda)$, or $s(\lambda)$ data, respectively. We calculate α_D from AATS-6 AOD spectra, α_E from $E(\lambda)$ derived from the ship in situ particle size measurements at AATS-6 wavelengths, and α_s from the ship nephelometer spectral measurements of total scattering. As noted by Quinn et al. (1998), the actual limits

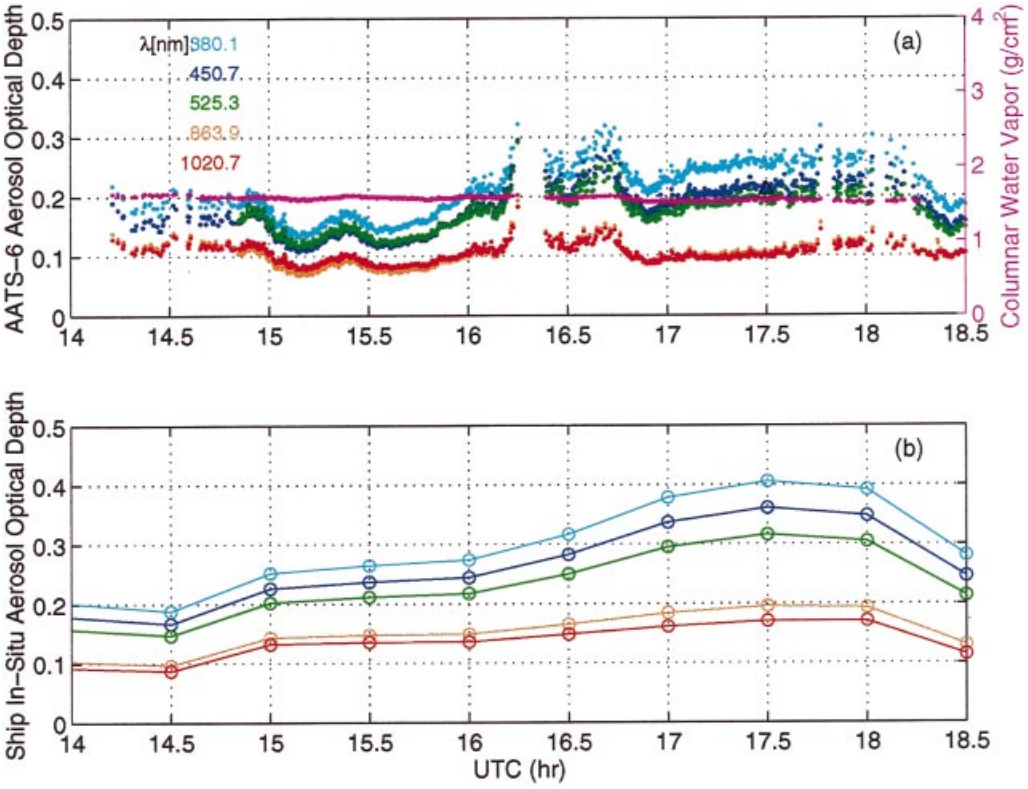

Fig. 11. (a) Marine boundary layer aerosol optical depth and columnar water vapor measured by AATS-6, columnar water vapor measured by radiosonde (triangle); (b) boundary layer aerosol optical depth calculated from shipboard in situ aerosol size distribution measurements for a refractive index of $1.40 - 0.0035i$ for 10 July 1997.

of integration over zenith angle are truncated within the nephelometer because of geometrical limitations. This angular truncation is most pronounced for supermicron particles, which preferentially scatter light in the forward direction. We note that no adjustment has been made to the nephelometer data to correct for this instrument angular truncation error, and this can result in calculated Ångström exponents that are too large, especially when scattering is dominated by large sea salt particles.

In previous studies (Von Hoyningen-Huene and Raabe, 1987; Reddy et al., 1990; Hoppel et al., 1990; Smirnov et al., 1994; Villevalde et al., 1994; Smirnov et al., 1995; Quinn et al., 1998), α has been used as an index to compare air masses with different aerosol signatures or merely to characterize the dependence of scattering on wavelength and hence on particle size. These studies led us to question whether α might be used to assess agreement between the shipboard in situ and sunphotometer measurements. We would expect agreement only for those cases where the MBL is well-mixed and the total atmospheric column AOD is dominated by the MBL aerosol. Like Reddy et al. (1990), we recognize that there is inherent error in the use of α because the shapes of the MBL/total columnar aerosol size distribution and the associated spectral extinction, scattering, or AOD curves are not necessarily well-represented by a power-law distribution.

Because total column AOD on 10 July appears to have been dominated by well-mixed aerosol within the MBL, we examine α values for this day in detail. Fig. 12a compares α values from the various instruments for the period 1200–1900 UTC. Values of α_D are shown for calculations performed for AATS-6 MBL AOD and for

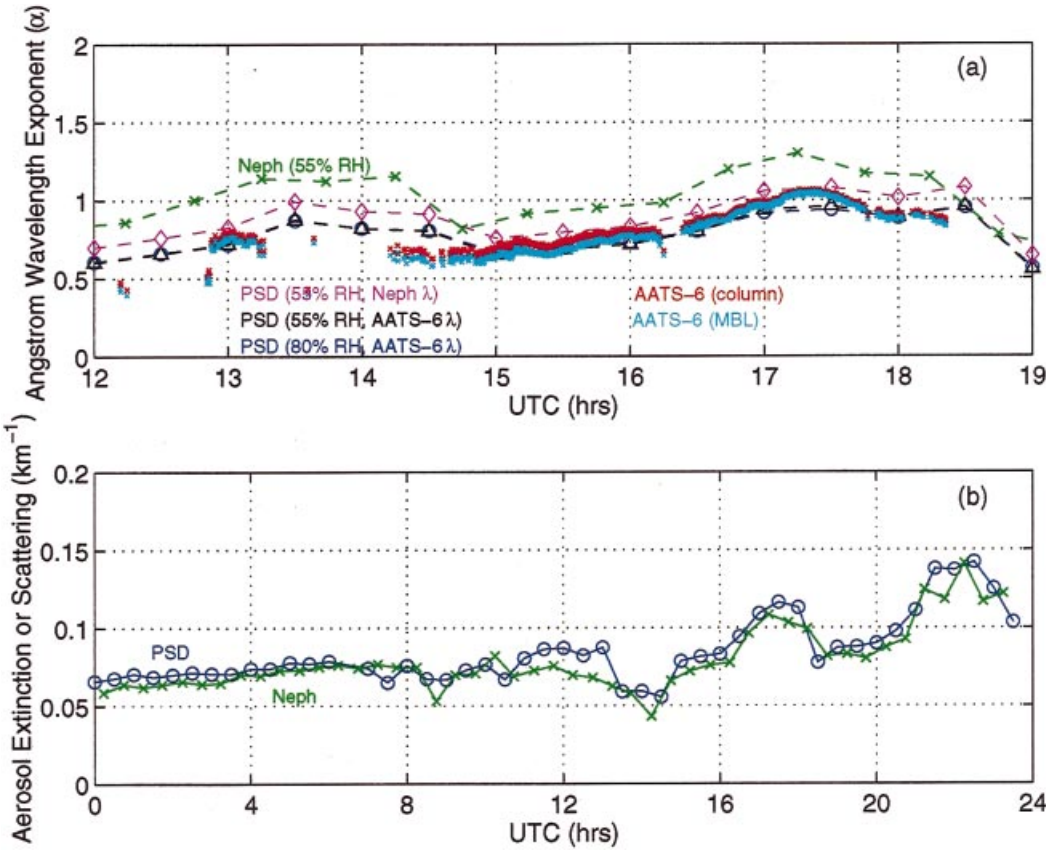

Fig. 12. For 10 July 1997: (a) comparison of Ångström wavelength exponent, α, calculated from AATS-6 MBL AODs (cyan) and from AATS-6 total column AODs (red), from extinction derived from shipboard aerosol size distribution measurements (PSD) at AATS-6 wavelengths for RH 55% (black triangles) and RH 80% (blue circles) and at nephelometer wavelengths for RH 55% (magenta diamonds), and from shipboard nephelometer measurements of particle scattering coefficient (green $\times$ symbols); and (b) comparison of aerosol extinction coefficients calculated at 550 nm from ship particle size data at RH 55% for a refractive index $1.40 - 0.0035i$ and from aerosol scattering coefficients measured by shipboard nephelometer at a sampling RH 55%.

AATS-6 total column AOD spectra. Three separate time series of α_E are shown to investigate the effect of choice of wavelengths on the α_E calculation. These include one each for $E(\lambda)$ calculated at the 5 AATS-6 AOD wavelengths and at the 3 nephelometer wavelengths for RH 80% (approximate ambient), and one for $E(\lambda)$ calculated at the 3 nephelometer wavelengths for RH 55% (the nephelometer sampling RH). A refractive index of $1.40 - 0.0035i$ was assumed in the $E(\lambda)$ calculations. The time series for α_s was calculated as described above. The magnitudes differ significantly, and the particle size distribution values do show some dependence on RH and on the range of specific wavelengths chosen for analysis. In general, however, the correlation appears very good for the 1500–1800 UTC time period. When total column α_D values are averaged over 30-min time periods, the $(\alpha_D - \alpha_s)$ rms difference is 0.20 with a bias of -0.19 ± 0.04. The analogous $(\alpha_D - \alpha_E)$ rms difference (for RH 80%) is 0.10, with a $(\alpha_D - \alpha_E)$ bias of 0.04 ± 0.09. Coefficients of determination, r^2, are 0.98 for α_s versus α_D and 0.60 for α_E versus α_D. The spectral dependence of the AATS-6 MBL AODs is slightly flatter than that of the AATS-6 total column AODs, as evidenced by α_D values that are 0.05–0.10 less than those derived from the total column AODs.

Fig. 12b compares values of 550-nm aerosol scattering coefficient measured by the nephelometer with corresponding extinction values calculated at 550 nm for a refractive index of $1.40 - 0.0035i$ from the ship height particle size measurements adjusted to the nephelometer sampling RH of 55%. Results are shown for the entire day. Differences between the calculated extinction and the measured scattering range from -0.01 to $+0.019\,km^{-1}$ (-12 to $+33\%$), with a mean difference of $0.005\,km^{-1}$ ($+7\%$). Results are essentially unchanged (to a precision of $0.001\,km^{-1}$) if a non-absorbing refractive index of $1.40 - 0i$ is assumed.

3.3. 22 July 1997

On 22 July, the R/V *Vodyanitskiy* sailed in a region located about 1.5° longitude off the Portugal coast and about 3° latitude and longitude northwest of Sagres. A large region of high pressure extended from the Azores to the North Sea (Verver et al., 2000) and resulted in outflow from western Europe on this day. Five-day backward trajectories indicate that air parcels below 850 hPa at the ship location were transported from the northern European continent west, then south through France, west over the ocean north of Spain, and then south to the ship. Ship radiosonde soundings at about 1100 and 1700 UTC indicated a weak subsidence inversion at 410–470 m and 320–400 m, respectively, with an estimated boundary layer top at 300 m at 1100 UTC and no definable layer at 1700 UTC.

Fig. 13a presents the time series of AATS-6 AOD and CWV measurements for this day. Due to ship heading and sun position relative to the ship, data prior to 1330 UTC were subject to frequent obscuration by shipboard wires/structures. However, the general temporal trend is still discernible. Peak values of AOD (about 0.25 at 525 nm) were measured just before noon, with a gradual decrease during the early afternoon, followed by a relative maximum (0.20 at 525 nm) at about 1500 UTC and lower relatively constant values (0.17 at 525 nm) from 1600 to 1800 UTC. No shipboard particle size data were available for the time period during which AATS-6 measurements were taken. Fig. 13b overplots α_D and α_s, with good agreement after 1300 UTC.

Lidar aerosol backscatter measurements ($\lambda = 532$ nm) during the period 1429–1739 UTC can be compared with the AATS-6 measurements. Lidar background- and range-corrected relative backscatter profiles are shown in Fig. 14a for 5 times. The data show significant aerosol backscatter returns up to 1.8 km, but the peak signals occur in the MBL below 350 m, which is consistent with the 1700 radiosonde data. Fig. 14b shows the corresponding extinction profiles derived from the lidar backscatter profiles by using the best estimate lidar system calibration constant and assuming height-dependent extinction-to-backscatter ratios calculated from the Ackermann (1998) continental aerosol model and the radiosonde RH profile. These profiles indicate a peak in the MBL aerosol extinction at 1518 UTC, with significant decreases after that time. Above the boundary layer, the aerosol backscatter and extinction structures are more complicated. Time-dependent lidar-derived AODs have been estimated by integrating each extinction profile after assuming a constant value of extinction coefficient within the overlap region below 120 m equal to the maximum derived value between 100 and 250 m. This procedure leads to optical depth errors on the order of $\pm 10\%$;

Table 3. *Aerosol optical depths measured by AATS-6 and derived from University of Munich lidar backscatter measurements taken from aboard the R/V* Vodyanitskiy *on 22 July*

LMU lidar AOD (532 nm)			AATS-6	
UTC	Continental	Marine	AOD (525 nm)	UTC
142945	0.199 ± 0.025	0.105 ± 0.017	0.183 ± 0.010	142820–143108
151810	0.206 ± 0.026	0.105 ± 0.017	0.187 ± 0.010	151647–151935
160747	0.160 ± 0.046	0.082 ± 0.030	0.165 ± 0.010	160622–160910
163248	0.179 ± 0.025	0.096 ± 0.016	0.161 ± 0.010	163121–163410
173837	0.183 ± 0.025	0.100 ± 0.016	0.160 ± 0.010	173711–173946

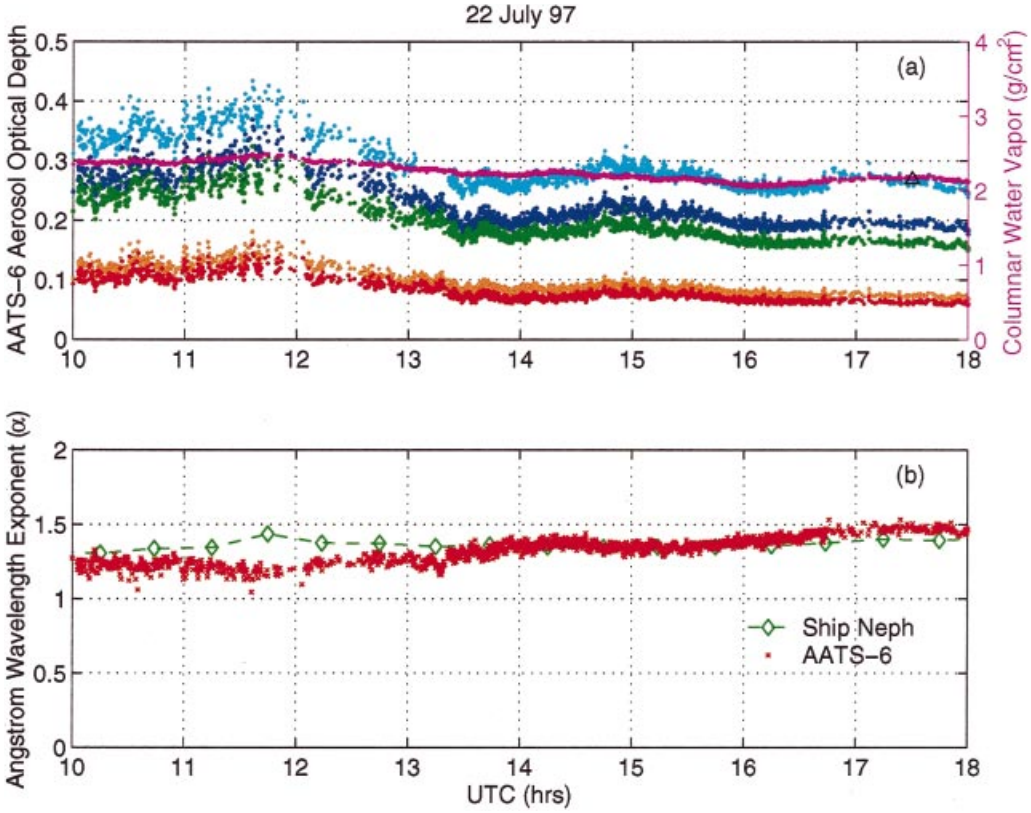

Fig. 13. For 22 July 1997: (a) columnar aerosol optical depth and water vapor measured by AATS-6, columnar water vapor measured by radiosonde (triangle); (b) comparison of Ångström wavelength exponent, α, calculated from AATS-6 column AODs and from shipboard nephelometer measurements of particle scattering coefficient at RH 55%.

additional errors of $\pm$10–20% can result from uncertainties associated with required profile splicing and overlap correction. Fig. 14c and Table 3 compare AODs calculated from the lidar-inferred extinction profiles for the Ackermann continental and marine aerosol extinction-to-backscatter models with coincident mean AATS-6 total column AODs calculated for 3-min time periods. The error bars on the lidar AODs are those due to calibration only; error bars on the AATS-6 AODs represent upper limit combined measurement and temporal variability uncertainties. In general, similar temporal behavior is observed, with a peak AATS-6 AOD at 525 nm of 0.187 at 1518 UTC, followed by a subsequent decrease to 0.160 at 1738 UTC. Consistent with the European source of the aerosol, lidar AOD results derived using the Ackermann continental aerosol extinction-to-backscatter model yield significantly better agreement with the AATS-6 values than do those derived using the marine aerosol model.

4. Summary and conclusions

Shipboard sunphotometer (AATS-6) measurements of AOD and CWV have been presented for a subset of the data collected during ACE-2. AATS-6 values of CWV have been shown to agree well with corresponding radiosonde measurements on several days and with airborne AATS-14 and UWPH measurements on 10 July. Detailed analyses of AATS-6 AOD measurements acquired on 10 and 22 July have been presented. Spatially and temporally coincident measurements of AOD by AATS-6 and AVHRR on 10 July have been com-

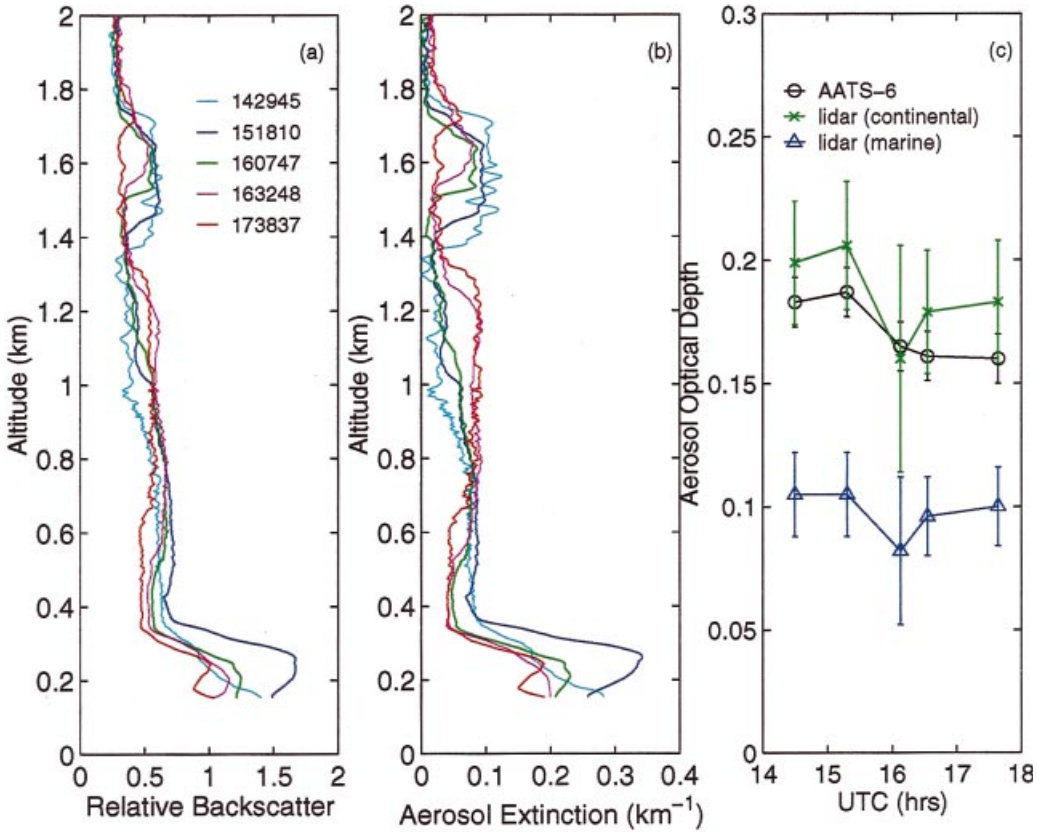

Fig. 14. For 22 July 1997: (a) shipboard lidar relative backscatter profiles at 532 nm, (b) corresponding aerosol extinction profiles derived from the relative backscatter profiles, (c) AATS-6 AOD at 525 nm and lidar-inferred AOD at 532nm.

pared, and AVHRR AODs were found to have exceeded corresponding mean AATS-6 AODs by about 0.04, which is greater than the estimated measurement uncertainties, although the uncertainty in the AVHRR AOD retrieval algorithm (Durkee et al., 2000) has yet to be quantified. AATS-14 AODs have also been presented for measurements taken from the Pelican at an altitude of about 60 m MSL at a location about 70 km from the ship 15 min prior to the NOAA-14 satellite overpass. Comparison of AATS-14 AODs with the corresponding AVHRR AODs calculated for the aircraft location indicates AVHRR values also exceeded the AATS-14 AODs by about 0.04. It is estimated that approximately 0.010–0.015 of this difference can be explained by AOD in the layer between the sea surface and the aircraft altitude. The remainder is attributed to temporal variations in the overlying aerosol between the times of the AATS-14 and AVHRR measurements.

An in-depth attempt to demonstrate column closure between measured AATS-6 MBL AODs and corresponding values calculated from shipboard in situ aerosol size distribution measurements on 10 July resulted in significant overestimates of AATS-6 measured AOD by the calculated AOD. In large part, we attribute these discrepancies to the high sensitivity of the closure methodology to models of hygroscopic growth, which have not been validated over the necessary range of particle size/composition distributions. Smaller differences were obtained by using more water-like refractive indices and, especially, particle growth factors that neglected the presence of sea salt measured at the ship. Our assumption that particle refractive index (hence, composition)

is constant with particle size, RH, and wavelength is not valid. Although our sensitivity studies with 3 refractive indices indicate that this chemical composition effect is less important than the particle size effect due to hygroscopic growth, the measurement-based size-segregated chemical composition modeling methodology of Collins et al. (2000) represents a significantly more rigorous and realistic approach that should be adopted in future studies.

Accurate characterization of the vertical distribution of aerosol is critical to the calculation of AOD from a single size distribution measurement, because extinction is directly proportional to the particle number density. Our assumption of constant particle number density up to the height of the peak in RH (i.e., equal mixing of all particles regardless of size) and then a linear decrease above that height may be incorrect and, in any event, is certainly not an ideal approach. Multiwavelength aerosol lidar backscatter measurements probably offer the best means for quantifying the vertical distribution of aerosol within the marine boundary layer because only lidar can provide an instantaneous, quantitative range-resolved view of the overlying atmosphere. However, calculation of aerosol extinction and optical depth from measurements taken by a zenith-pointing aerosol backscatter lidar requires that the lidar be well-calibrated, that pulse-to-pulse variations in transmitted energy variations be known and accounted for, and that signal degradation due to incomplete overlap between the transmitted and received laser beams at ranges near the lidar can be accurately characterized and corrected. Moreover, the extinction-to-backscatter ratio, which depends on both particle size and composition (hence RH and aerosol type) must be known throughout the aerosol layer. Achieving all these proved difficult aboard the ship; additional analysis of the lidar data set may lead to a better quantification of errors and permit additional comparisons.

Because the Ångström wavelength exponent, α, has been used often in previous studies both as a measure of particle size and to characterize the origin of air masses, we have examined the spectral dependence of AATS-6 AOD measurements by calculating time-dependent values of α_D from the instantaneous total column AODs. Comparisons have been made of AATS-6 α_D values with corresponding values, α_E, derived for the ship height from particulate extinction calculated for a refractive index of $1.40 - 0.0035i$ from shipboard in situ measurements of aerosol size distribution adjusted for hygroscopic particle growth, and with values, α_s, calculated from nephelometer total particle scattering measurements at 55% RH. Fig. 15 summarizes the results of our calculations for portions of 9 days by showing scatter plots of α_E versus α_D (Fig. 15a) and α_s versus α_D (Fig. 15b). Data have been segregated by air mass source region according to the classification scheme of Quinn et al. (2000). The results are highly variable among the cases. For the composite data set, the rms difference for $(\alpha_s - \alpha_D)$ is 0.32, with a bias of 0.10, and the rms difference for $(\alpha_E - \alpha_D)$ is 0.50, with a bias of -0.10. Several factors might have contributed to the high degree of variability in the results. These include incorrect optical modeling of the aerosol size distribution through use of a size- and wavelength-independent refractive index, poorly known/modeled hygroscopic growth of supermicron particles, use of different wavelength regions sampled by the instruments to calculate α, underestimates of large particle contributions to total scattering that result from truncation of angular integration limits within the nephelometer, presence of particle absorption not accounted for in the nephelometer total scattering measurements, variations in the vertical distribution and optical properties of a mixed clean marine and polluted continental aerosol within the boundary layer, and significant contributions to AOD from aerosol above the well-mixed layer (although none of the cases we analyzed included a Saharan dust layer). These results illustrate further the great difficulty of deriving column values from point measurements.

5. Acknowledgments

This research was conducted as part of the 2nd Aerosol Characterization Experiment (ACE-2), which is a contribution to the International Global Atmospheric Chemistry (IGAC) core project of the International Geosphere-Biosphere Programme (IGBP). Financial support for the measurements and analyses was provided by the US National Oceanic and Atmospheric Administration, Office of Naval Research, National Aeronautics and Space Administration,

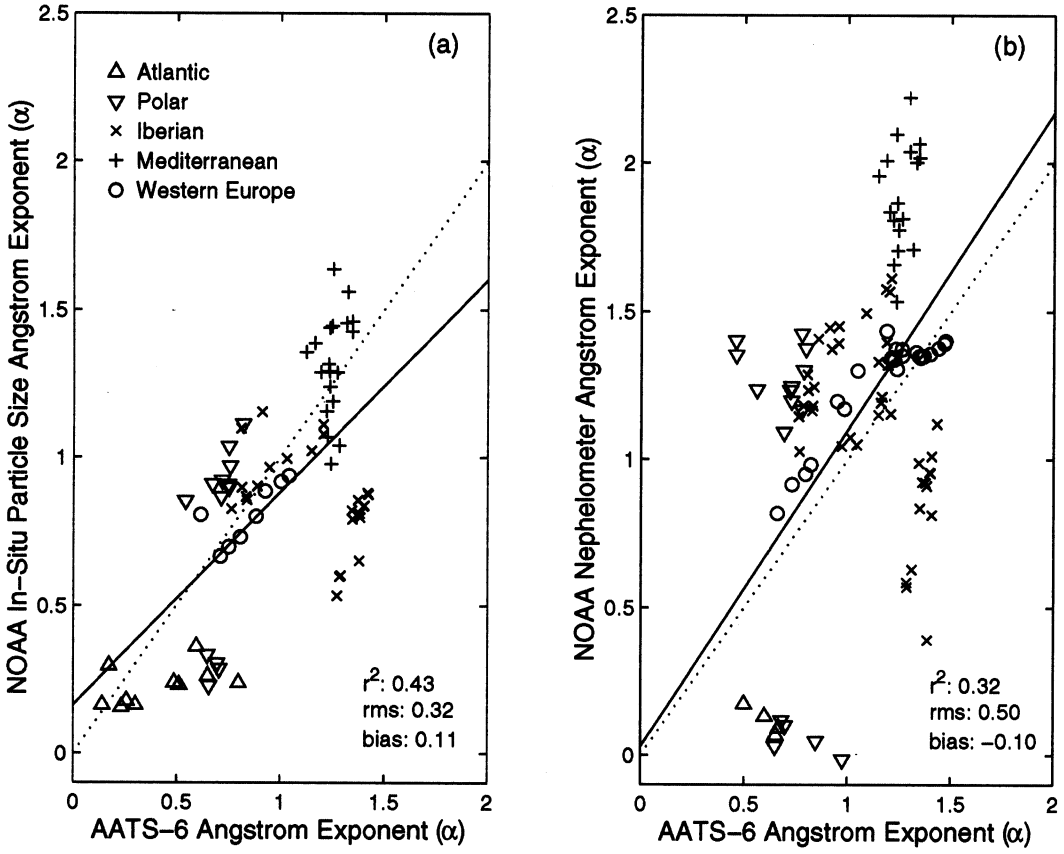

Fig. 15. Scatter diagrams of Ångström wavelength exponents calculated from (a) aerosol extinction spectra derived from shipboard particle size measurements and (b) shipboard nephelometer scattering measurements versus Ångström exponents calculated from AATS-6 total column AOD measurements acquired during portions of 9 days during ACE-2. Data have been segregated by air mass source region according to the classification scheme of Quinn et al. (2000). The solid lines represent the regression fits, and the dotted lines one-to-one correspondence.

and the European Commission DG XII (Environment and Climate). We thank the Ozone Processing Team at NASA Goddard Space Flight Center for making available TOMS Earth Probe ozone data.

REFERENCES

Ackermann, J. 1998. The extinction-to-backscatter ratio of tropospheric aerosol: a numerical study. *J. Atmos. and Oceanic Technol.* **15**, 1043–1050.

Bates, T. S., Quinn, P. K., Covert, D. S., Coffman, D. J., Johnson, J. E. and Wiedensohler, A. 2000. Aerosol physical properties and controlling processes in the lower marine boundary layer: a comparison of sub-micron data from ACE-1 and ACE-2. *Tellus* **52B**, 258–272.

Collins, D. R., Jonsson, H. H., Seinfeld, J. H., Flagan, R. C., Gassó, S., Hegg, D. A., Russell, P. B., Schmid, B., Livingston, J. M., Öström, E., Noone, K. J., Russell, L. M. and Putaud, J. P. 2000. In situ aerosol size distributions and clear column radiative closure during ACE-2. *Tellus* **52B**, 498–525.

Durkee, P. A., Nielsen, K. E., Russell, P. B., Schmid, B., Livingston, J. M., Collins, D., Flagan, R. C., Seinfeld, J. H., Noone, K. J., Öström, E. Gassó, S., Hegg, D.,

Bates, T. S. and Quinn, P. K. 2000. Regional aerosol properties from satellite observations: ACE-1, TARFOX and ACE-2 results. *Tellus* **52B**, 484–497.

Gassó, S., Hegg, D., Noone, K., Covert, D., Schmid, B., Russell, P., Livingston, J., Durkee, P. and Jonsson, H. 2000. Optical and hygroscopic aerosol properties in the west subtropical Atlantic, and their contribution to the upwelling radiance. *Tellus* **52B**, 546–567.

Hänel, G. 1976. The properties of atmospheric aerosol particles as functions of the relative humidity at thermodynamic equilibrium with the surrounding moist air. *Adv. Geophys.* **19**, 77–188.

Hoppel, W. A., Fitzgerald, J. W., Frick, G. M. and Larson, R. E. 1990. Aerosol size distributions and optical properties found in the marine boundary layer over the Atlantic Ocean. *J. Geophys. Res.* **95**, 3659–3686.

Johnson, J. E., Koropalov, V. M., Pickering, K. E., Thompson, A. M., Bond, N. and Elkins, J. W. 1993. Third Soviet-American Gas and Aerosol (SAGA-3) experiment: overview and meteorological and oceanographic conditions. *J. Geophys. Res.* **98**, 16,893–16,908.

Johnson, D., Osborne, S., Wood, R. Suhre, K., Johnson, R., Businger, S., Quinn, P. K., Durkee, P., Russell, L. M., Andreae, M. O., O'Dowd, C., Noone, K. J., Bandy, B., Rapsomanikis, S. and Rudolph, J. 2000. An overview of the Lagrangian experiments undertaken during the north Atlantic regional Aerosol Characterization Experiment (ACE-2). *Tellus* **52B**, 290–320.

Livingston, J. M. and Russell, P. B. 1989. *Comparison of satellite-inferred (SAGE II) AODs with corresponding airborne sun-photometer optical depths*. Preprint AIAA 27th Aerospace Sciences Meeting, January 9–12, 1989, Reno, Nevada.

Livingston, J. M. and Russell, P. B. 1997. AOD spectra, vertical profiles, and horizontal transects derived from TARFOX airborne sunphotometer measurements. EOS. *Trans. Amer. Geophys. Union* **78**, S92.

Matsumoto, T., Russell, P. B., Mina, C. and Van Ark, W. 1987. Airborne tracking sunphotometer. *J. Atmos. Oceanic Technol.* **4**, 336–339.

Michalsky, J. J., Liljegren, J. C. and Harrison, L. C. 1995. A comparison of sun photometer derivations of total column water vapor and ozone to standard measures of same at the Southern Great Plains Atmospheric Radiation Measurement site. *J. Geophys. Res.* **100**, 25,995–26,003.

Pueschel, R. F. and Livingston, J. M. 1990. Aerosol spectral optical depths: jet fuel and forest fire smokes. *J. Geophys. Res.* **95**, 22,417–22,422.

Quinn, P. K., Coffman, D. J., Kapustin, V. N., Bates, T. S. and Covert, D. S. 1998. Aerosol optical properties in the marine boundary layer during the first Aerosol Characterization Experiment (ACE-1) and the underlying chemical and physical aerosol properties. *J. Geophys. Res.* **103**, 16,547–16,563.

Quinn, P., Coffman, D. J., Bates, T. S. and Covert, D. S. 2000. Chemical and optical properties of ACE-2 aerosol. *Tellus* **52B**, 239–257.

Raes, F., Bates, T. and McGovern, F. 2000. The second Aerosol Characterization Experiment (ACE-2): general overview and main results. *Tellus* **52B**, 111–126.

Reddy, P. J., Kreiner, F. W., DeLuisi, J. J. and Kim, Y. 1990. Aerosol optical depths over the Atlantic derived from shipboard sunphotometer observations during the 1988 Global Change Expedition. *Global Biochem. Cycles* **4**, 225–240.

Russell, P. B. and Heintzenberg, J. 2000. An overview of the ACE-2 clear sky column closure experiment (CLEARCOLUMN). *Tellus* **52B**, 463–483.

Russell, P. B., Livingston, J. M., Pueschel, R. F., Reagan, J. A., Browell, E. V., Toon, G. C., Newman, P. A., Schoeberl, M. R., Lait, L. R., Pfister, L., Gao, Q. and Herman, B. M. 1993. Post-Pinatubo optical depth spectra vs. latitude and vortex structure: airborne tracking sunphotometer measurements in AASE II. *Geophys. Res. Lett.* **20**, 2571–2574.

Russell, P. B., Hobbs, P. V. and Stowe, L. L. 1999a. Aerosol properties and radiative effects in the United States east coast haze plume: an overview of the Tropospheric Aerosol Radiative Forcing Observational Experiment (TARFOX). *J. Geophys. Res.* **104**, 2213–2222.

Russell, P. B., Livingston, J. M., Hignett, P., Kinne, S., Wong, J. and Hobbs, P. V. 1999b. Aerosol-induced radiative flux changes off the United States mid-Atlantic coast: comparison of values calculated from sunphotometer and in situ data with those measured by airborne pyranometer. *J. Geophys. Res.* **104**, 2289–2307.

Scheele, M. P., Siegmund, P. C. and Van Velthoven, P. F. J. 1997. Sensitivity of trajectories to data resolution and its dependence on the starting point: in or outside a tropopause fold. *Meteor. Appl.* **3**, 267–273.

Schmid, B., Thome, K. J., Demoulin, P., Peter, R., Matzler, C. and Sekler, J. 1996. Comparison of modeled and empirical approaches for retrieving columnar water vapor from solar transmittance measurements in the 0.94-mm region. *J. Geophys. Res.* **101**, 9345–9358.

Schmid, B., Livingston, J. M., Russell, P. B., Durkee, P. A., Jonsson, H. H., Collins, D. R., Flagan, R. C., Seinfeld, J. H., Gassó, S., Hegg, D. A, Öström, E., Noone, K. J., Welton, E. J., Voss, K., Gordon, H. R., Formenti, P. and Andreae, M. O. 2000. Clear sky closure studies of lower tropospheric aerosol and water vapor during ACE-2 using airborne sunphotometer, airborne in-situ, space-borne, and ground-based measurements. *Tellus* **52B**, 568–593.

Smirnov, A., Royer, A., O'Neill, N. T. and Tarussov, A. 1994. A study of the link between synoptic air mass type and atmospheric optical parameters. *J. Geophys. Res.* **99**, 20,967–20,982.

Smirnov, A., Villevalde, Y., O'Neill, N. T., Royer, A. and Tarussov, A. 1995. Aerosol optical depth over the oceans: analysis in terms of synoptic air mass types. *J. Geophys. Res.* **100**, 16,639–16,650.

Swietlicki, E., Zhou, J., Berg, O. H., Hameri, K.,

Vakeva, M., Makela, J., Covert, D. S., Dusek, U., Busch, B., Wiedensohler, A. and Stratmann, F. 2000. Hygroscopic properties of aerosol particles in the eastern Northern Atlantic during ACE-2. *Tellus* **52B**, 201–227.

Tang, I. N. 1996. Chemical and size effects of hygroscopic aerosol on light scattering coefficients. *J. Geophys. Res.* **101**, 19,245–19,250.

Tanre, D., Kaufman, Y. J., Herman, M. and Mattoo, S. 1997. Remote sensing of aerosol properties over oceans using MODIS/EOS spectral radiances. *J. Geophys. Res.* **102**, 16,971–16,988.

Tomasi, C., Marani, S., Vitale, V., Cacciari, A. and Lupi, A. 2000. Precipitable water evaluations from infrared sun-photometric measurements analyzed using the atmospheric hygrometry technique. *Tellus* **52B**, 734–749.

Verver, G., Raes, F., Vogelenzang, D. and Van Liedekerke, M. 2000. The 2nd Aerosol Characterization Experiment (ACE-2): meteorological and chemical overview. *Tellus* **52B**, 126–140.

Vitale, V., Tomasi, C., Bonafe, U., Marani, S., Lupi, A., Cacciari, A. and Ruggeri, P. 2000. Spectral measurements of aerosol particle extinction in the 0.4–3.7 μm wavelength range, performed at Sagres with the IR-RAD sun-radiometer. *Tellus* **52B**, 716–733.

Villevalde, Y. V., Smirnov, A. V., O'Neill, N. T., Smyshlyaev, S. P. and Yakovlev, V. V. 1994. Measurement of aerosol optical depth in the Pacific Ocean and the North Atlantic. *J. Geophys. Res.* **99**, 20,983–20,988.

Von Hoyningen-Huene, W. and Raabe, A. 1987. Maritime and continental air mass differences in optical aerosol extinction data. *Contrib. Atmos. Phys.* **60**, 81–87.

Wiegner, M., Quenzel, H., Rabus, D., Volker, W., Volger, P., Ackermann, J., Kahler, C., Fergg, F. and Wildgruber, G. 1995. The Mobile Three-Wavelength Backscatter Lidar of the Meteorological Institute of the University Munich, Lidar and Atmospheric Sensing. *SPIE* **2505**, 2–10.